

CONFIDENTIAL

DECLASSIFIED

NATIONAL AERONAUTICS AND SPACE ADMINISTRATION

TECHNICAL MEMORANDUM X-493

AFTERBODY HEATING DATA OBTAINED FROM AN ATLAS-BOOSTED
MERCURY CONFIGURATION IN A FREE BODY REENTRY*

By Emily W. Stephens

SUMMARY

An Atlas-boosted capsule was flight tested in an effort to substantiate design information for the Project Mercury capsule as well as for reentry bodies in general. This report summarizes the afterbody heating data determined from measurements made on the capsule during atmospheric reentry at near satellite velocities.

Detailed examination of the recovered capsule revealed little thermal damage on the conical afterbody, although indication of skin buckling due to excessive heating was clearly visible on the cylindrical section. Measured temperatures showed that peak heating occurred on the cylindrical section where a maximum temperature of 2,260° F was recorded and a peak heating rate of 27.5 Btu/ft²-sec was encountered.

The jet control system, which was intended to orient and control the capsule attitude, was inoperable during reentry because of a delayed capsule-booster separation. As a result, the capsule reentered the atmosphere at a high angle of attack as an oscillatory free body.

INTRODUCTION

With the advent of Project Mercury, new design concepts were introduced for a vehicle which could support manned orbital flight. Full-scale free-flight test data were needed to obtain the design information for such a vehicle. In order to obtain some of these data, a capsule, designated "Big Joe," was designed to explore the

* Title, Unclassified.

DECLASSIFIED - EFFECTIVE 1-15-64
Authority: Memo Geo. Drobka NASA HQ.
Code ATSS-A Dtd. 3-12-64 Subj: Chang
in Security Classification Markings

12699

Authn

03710391000

2

heating environment associated with atmospheric reentry from a shallow earth orbit.

A general discussion of the Big Joe flight has been presented in reference 1 and the ablation heat shield performance during reentry has been discussed in reference 2. This report summarizes the heat-transfer results obtained along the afterbody during the reentry phase of the flight trajectory.

The capsule was launched from the U.S. Air Force Missile Test Center, Cape Canaveral, Florida, on September 9, 1959, at 2:19 a.m., e.s.t. and was recovered approximately 1,300 nautical miles downrange 7 hours after launch.

SYMBOLS

h	altitude, ft
M	Mach number
N_{St}	Stanton number
N_{Pr}	Prandtl number
p	dynamic pressure, lb/ft^2
q	heating rate, $Btu/ft^2\text{-sec}$
R	Reynolds number
T	temperature, $^{\circ}F$
t	time, sec
V	velocity, ft/sec
α	angle of attack, deg

Subscripts:

D	diameter, ft
∞	free-stream condition

2 body length, ft

An asterisk denotes properties evaluated at reference temperature or enthalpy.

INSTRUMENTATION AND TRAJECTORY OF TEST VEHICLE

Capsule Description

The geometric configuration of the test capsule is presented in the detailed sketch and photographs of figures 1 to 4. The external dimensions were essentially the same as the Project Mercury capsule although the structural details were not typical of the Mercury design.

The capsule center of gravity was offset laterally from the center line by 0.6 inch and vertically by 0.15 inch. (See fig. 1.) This offset caused the capsule to trim about an angle of between 5° and 6° .

The capsule afterbody was constructed and assembled in four sections as shown in figure 2. The pressurized compartment contained the instrumentation shown in figure 3. The antenna elements for the telemetry system and radar beacons (see fig. 2) were located on the conical section which together with the cylindrical section housed the main parachute. The top canister contained the drogue parachute. The pressure vessel sidewalls were constructed of 0.062-inch sheet Inconel. Between stations 6.02 and 26.08 (see fig. 1) the inside wall of the pressure vessel was insulated by a 2-inch layer of 7 lb/cu ft Thermoflex separated from the pressure vessel sidewall by a $\frac{1}{4}$ -inch air gap. The conical and cylindrical afterbodies and canister were constructed of 0.050-inch, 0.032-inch, and 0.032-inch sheets of corrugated Inconel, respectively. The orientation of the skin corrugations is shown in figure 2. A fiber-glass lid was used to cover the blunt face of the canister to provide heat protection during exit. Hooks for use in recovering the capsule were attached to the cylindrical section. (See fig. 2.)

Instrumentation

The capsule was instrumented to obtain measurements of heating, angular rates, accelerations, and sound and vibration. Capsule afterbody temperatures were measured by 52 chromel-alumel thermocouples arranged as shown in figure 5. Of the total of 52 thermocouples

located on the afterbody, 41 were installed to obtain convective heating data. The remaining 11 thermocouples were provided primarily to measure internal and structural temperatures. The thermocouple locations and wall thicknesses are tabulated in table I for the 41 thermocouples which are discussed in this report. The thermocouples were installed by spot welding to the inner surface of the skin with the exception of thermocouples 16 and 53, which were embedded in holes bored in the fiber-glass canister lid. The main lines of thermocouples were located on the flat areas between skin corrugations. The thermocouples were arranged along the span of the capsule in three rows, equidistantly spaced, in an attempt to detect any asymmetrical heating which might occur.

The outputs from these thermocouples with three reference voltages were commutated and transmitted on an FM/FM, 20-watt radio frequency telemetry link. The commutation rate was such that temperatures at any given station were sampled about once every 0.62 second. The reference voltages provided an in-flight calibration of the thermocouple system. Maximum error in the temperature measurements was estimated to be within $\pm 30^\circ$.

Telemeter data were not obtained during the period of ionization blackout of the signal which occurred over the period of 480 to 570 seconds. The data for this time interval were stored on an onboard magnetic tape recorder and played back after the capsule was recovered.

Temperature-sensitive paint was applied to the inside of the skin to substantiate thermocouple measurements. This paint provided an approximate method of determining the maximum temperatures attained by the skin.

Trajectory

Since no reentry trajectory was obtained from radar tracking data, it was necessary to calculate a trajectory. The initial conditions were obtained from a small amount of midcourse radar data (time histories of altitude, velocity, and flight-path angle) obtained near the end of powered flight. The trajectory shown in figure 6 was calculated by matching, as accurately as possible, the time history of the average longitudinal accelerations, recorded during the reentry phase of the flight, with calculated values obtained by using drag coefficients from reference 3 and density based on the 1959 ARDC atmosphere (ref. 4). A three-degree-of-freedom point-mass program which assumed zero lift was used in calculating the trajectory.

DECLASSIFIED

5

FLIGHT TEST

The Big Joe capsule was launched from the U.S. Air Force Missile Test Center, Cape Canaveral, Florida, on September 9, 1959. The Atlas missile 10-D was employed to boost the capsule to an altitude of 491,320 feet at a path angle of -0.92° relative to the local horizon and a corresponding velocity of 20,628 feet per second at sustainer engine burnout.

G
5
The Atlas booster engines failed to separate at staging and the added weight penalty during sustainer burning prevented the Atlas from attaining the desired insertion conditions. Since the desired insertion conditions were not attained, no sustainer engine cutoff signal was sent to the Atlas booster and thus the sustainer and vernier engines operated until all fuel was expended from the tank. However, some thrust was acting on the capsule following sustainer burnout because of residual fuel and/or oxygen in the tanks. As a result, capsule separation from the booster was delayed beyond the nominal sustainer burnout time until approximately 448 seconds.

The capsule control system was designed to generate a pitchover maneuver at a prescribed separation time and maintain the capsule attitude, heat shield foremost, during reentry. By the time the capsule and booster separation occurred, the control system had depleted its gas supply in attempting to orient the capsule-booster combination. The capsule was oriented solely by aerodynamic forces after booster separation, and a successful reentry, with heat shield forward, was attained without the aid of a control system.

As has been described in the section entitled "Capsule Description," an offset in the capsule center of gravity caused the capsule to trim about an angle of between 5° and 6° . Figure 7 presents the oscillatory amplitude about trim as a function of time. The capsule motions are not planar and the maximum and minimum values shown represent the extremes encountered. The frequency of the oscillation is shown in figure 8.

The capsule recovery system utilized a drogue stabilization parachute and a main parachute which were deployed at approximately 42,000 feet and 10,000 feet, respectively. The capsule was successfully recovered 7 hours after launch.

03171030 1000



RESULTS AND DISCUSSION

Although many facets of design interest were investigated in the Big Joe flight test, this report is concerned only with afterbody heating on the capsule during reentry.

Description of Recovered Capsule


The recovered capsule was carefully examined to determine any damage which might have occurred due to excessive heating. Little evidence of thermal damage was apparent on the conical afterbody, and no indications of local hot spots were found around such areas as the control jet openings on the pressure vessel, or on small protuberances such as rivet heads, antenna and skin joints, or structural corrugations.

Most of the thermal damage occurred on the cylindrical section where evidence of skin buckling was clearly visible. (See fig. 9(a).) The buckling did not extend around the entire circumference but was confined to the vicinity of the thermocouples designated as row A. Examination revealed that the buckling occurred only at the midspan position of the cylinder and did not extend fore or aft. Two of the three recovery hooks, which were equidistantly spaced around the top of the cylinder, showed extensive damage and the skin near the hooks was partially eroded. The damage to the recovery hooks may be seen in the photographs of figures 9(b) and 9(c). The damaged hooks were located on either side of row A, whereas no appreciable damage was found to exist on the third recovery hook which was located on the opposite side of the cylinder from row A. The unsymmetrical heating which existed on the afterbody may be attributed to capsule oscillations and the trim angle caused by the center-of-gravity offset. The concentration of damage to the vicinity of row A indicates that this side was windward during most of the heating.

Afterbody Temperatures and Heating Rates

Plots of afterbody temperatures and heating rates obtained during reentry heating against both time and wetted distance from the capsule shoulder are presented. Time histories are presented from burnout to drogue deployment. Peak temperatures, shown in the temperature time histories of figure 10, occur between 560 and 580 seconds.

The average pressure vessel sidewall peak temperatures along rows A, B and C (fig. 10(a)) are 753° F, 503° F, and 581° F, respectively.



The value for row A is approximately 250° higher than the average peak temperature measured on row B and 175° higher than that measured on row C. This variance in afterbody heating may be attributed to the nonzero incidence condition which existed during reentry.

Maximum temperatures recorded on the capsule afterbody were 830° F on the pressure vessel, $1,060^{\circ}$ F on the cone sidewall, $1,820^{\circ}$ F on the top canister, and $2,260^{\circ}$ F on the cylinder. Relatively little temperature rise was noted by thermocouples 16 and 53 which were embedded 0.125 inch in the fiber-glass lid of the canister (see fig. 5). The highest temperatures recorded on the afterbody are observed to be near the midspan position of the cylinder coincident with the area of buckling and on the canister. (See figs. 10(c) and 10(d).)

Temperature distributions along the capsule are presented in figure 11 at selected times during reentry. The reader is cautioned not to compare temperature levels of adjacent structural assemblies as an indication of relative heating rates because of the difference in local emissivity, wall thickness, and the structural contour of the skin.

The internal skin of the capsule afterbody was painted with a temperature-sensitive paint in an effort to substantiate the maximum temperatures measured by the thermocouples. The probable maximum temperatures estimated from the paint are presented in figure 12. Since the application of the paint was such that only approximate results could be obtained, the agreement between the temperatures measured by thermocouples and by temperature-sensitive paint was considered to be reasonable.

Slopes from the temperature time histories of figure 10 were utilized in evaluating the heating rates which are presented in figure 13. The temperature gradient through the skin for even the most severe heating rate was calculated to be less than 1° . The heating rates shown were obtained during oscillatory conditions and represent average values for the oscillatory motions shown in figure 7. Emissivity values used in the heating-rate calculations were 0.9 for the black painted surface of the pressure vessel and 0.6 for the corrugated sidewalls which extended over the remainder of the capsule, with the exception that laboratory-measured emissivity values (see fig. 14) were used in the calculations for thermocouples 12 and 13. The laboratory tests showed little variation of emissivity with temperature below $1,800^{\circ}$ F. Higher temperatures than this were obtained only on thermocouples 12 and 13.

In general, peak heating rates occur between 540 and 565 seconds. The values of the peak heating rates for various portions of the

03:41:20:18:30

afterbody are summarized as follows:

Location	Row	Time, sec	Max. q , Btu/ft ² -sec
Pressure vessel sidewall	A	565	5.1
Cone sidewall	A	550	5.1
Cylinder	A	558	27.5
Top canister	A	550	14.2

The local heating rates are presented in figure 15 as a function of the wetted distance from the capsule shoulder in inches. The heating-rate distributions are given from 520 to 570 seconds. Comparisons of the data from rows A, B, and C show that the heating rates along row A are for the most part higher than those along rows B or C. As discussed earlier, a physical examination of the recovered capsule also showed evidence of maximum heating along row A.

Figure 15 shows that the heating rates were reasonably uniform over the pressure vessel and conical afterbody from stations 8 to 64. A large increase in local heating rate occurs downstream of the cone-cylinder junction (station 64). It is not clear as to the exact mechanism which produced the high heating rates at station 74. (See figs. 15(b), 15(c), 15(d), and 15(e).) However, the flow is believed to reattach with a possible transition to turbulent flow in this region. Flow separation around the corner at the cylinder-canister step and reattachment on the canister is suggested by the data of figures 15(b) and 15(c). This distribution of heating rates is qualitatively similar to that obtained from wind-tunnel tests. (See ref. 5.) However, the data obtained along the top canister at 560 and 570 seconds does not follow previous trends. The characteristic low heating near station 90 followed by higher heating near station 104 is reversed.

It may be noted that heating rates obtained near the junction of the pressure vessel and the conical afterbody are slightly lower than the average level of heating rates over these sections. This effect is due to an uncorrected conduction error due to a heat-sink effect. This heat-sink effect results from a concentration of mass in this region which is needed to provide for mechanical connection of the airframe.

DECLASSIFIED

9

Stanton Numbers

Figure 16 presents local heat-transfer coefficients in nondimensional form as a function of free-stream Reynolds number. These Stanton numbers were based on free-stream aerodynamic conditions, faired heating rates from figure 13, and the difference between the adiabatic wall enthalpy and the enthalpy obtained at wall temperature. The recovery factor used in the data reduction was assumed to be 0.9.

Flight times are indicated along the abscissa of figure 16 to aid in interpreting the data. The heating-rate time histories of figure 13 indicate that significant afterbody heating occurs as early as 470 seconds ($R_{\infty,D} \approx 10^3$). Stanton numbers at $R_{\infty,D} \approx 10^3$ were of the order of 0.1 for the entire afterbody. A decreasing trend of Stanton number as a function of $R_{\infty,D}$ was found to be representative at all stations for $R_{\infty,D}$ up to approximately 5×10^5 .

Comparison of the heating-rate histories of figure 13 indicates that the maximum rates on the cylinder were 2 to 6 times higher than the maximum rates obtained on the conical section. It appears that this effect is due to laminar heating on the conical section followed by a transition to turbulent flow in the vicinity of the cone-cylinder junction. Figure 17 shows a comparison of Big Joe nondimensionalized heat-transfer coefficients measured at several representative stations with both laminar and turbulent theoretical Stanton numbers. The theoretical flat-plate turbulent values were determined by the Schultz Grunow turbulent skin-friction relation and the modified Reynolds analogy:

$$N_{St}^* = \frac{.185}{(\log_{10} R^*)^{2.584}} (N_{Pr}^*)^{-\frac{2}{3}}$$

and the laminar Stanton numbers were based on the laminar flat-plate skin-friction relation for attached flow and are also shown as modified for separated flow by the calculation of reference 6.

It should be noted that figure 17 differs from figure 16 in that properties are evaluated based on local pressures estimated from zero angle-of-attack wind-tunnel data and the reference enthalpy method of Eckert. (See ref. 7.) The reference lengths used in the Reynolds numbers were measured from the stagnation point for stations on the pressure vessel sidewall and conical section and from the cone-cylinder junction for the midcylinder position. These lengths were the same as those used in reference 8 for this configuration.

03:17:29.1030

10

Although the capsule was known to oscillate over the time period covered in figure 17 (500 to 580 seconds), reasonable agreement is obtained between measured Stanton numbers computed at zero angle of attack and theory, with the exception of thermocouple 12. The curves of figures 17(a) and 17(b) suggest the flow to be laminar on the pressure vessel sidewall and conical section for Reynolds numbers R_L^* less than approximately 2×10^4 and may approach turbulent flow at Reynolds numbers slightly greater than this. At the midcylinder position (fig. 17(c)), peak measured values on the windward side (thermocouple 12) exceed the predicted turbulent values by a factor of two. Also shown for comparison with Big Joe data in figure 17(c) are turbulent wind-tunnel data measured at $\alpha = 0^\circ$.

Calculations presented in reference 8 have suggested that the high Stanton numbers determined from thermocouple 12 are unlikely to be entirely an effect of angle of attack. However, since these Stanton numbers were obtained from a thermocouple which exceeded its calibrated range, some question exists as to the exact magnitude of the peak. Nevertheless, no doubt exists that the cylinder heating was considerably higher than early predictions based on separated laminar flow on the afterbody.

SUMMARY OF RESULTS

Afterbody temperatures were measured on the Big Joe, Atlas-boosted capsule under conditions simulating reentry from a shallow earth orbit. Although the missile did not attain the desired insertion conditions, much valuable design information was obtained from the flight test that is applicable to Project Mercury and reentry satellites in general. The following results were obtained:

1. Only slight thermal damage was found on the recovered capsule and no indications of local hot spots were found around such areas as the control jet openings on the pressure vessel, or on small protuberances such as rivet heads, antenna and skin joints, or structural corrugations. Some skin buckling, due to excessive localized heating, was apparent on the cylindrical section, and the large protruding hooks located on the cylinder were highly eroded.

2. Heating rates obtained from temperature time histories showed the highest heating rates occurred on the capsule cylindrical section and a maximum value of $27.5 \text{ Btu/ft}^2\text{-sec}$ was calculated. A maximum temperature of $2,260^\circ \text{ F}$ was recorded near the midspan of the cylindrical section. Heating rates were obtained over a free-stream Reynolds

DECLASSIFIED

11

number range from 1×10^3 to 1.5×10^6 .

3. An asymmetrical heating condition existed on the capsule afterbody due to the nonzero incidence which existed during reentry.

4. Stanton numbers obtained from flight results show reasonable agreement with theory. Measured values obtained on the pressure vessel sidewall and conical section agree well with laminar skin-friction data except at high Reynolds numbers. Both wind-tunnel and theoretical data failed to predict the high heating on the windward side of the cylinder.

Space Task Group,
National Aeronautics and Space Administration,
Langley Field, Va., January 25, 1961.

031712381030

12

REFERENCES

1. Bond, A. C., and Kehlet, A. B.: Review, Scope, and Recent Results of Project Mercury Research and Development Program. Paper No. 60-35, Inst. Aero. Sci., Jan. 1960.
2. O'Neal, Robert L., and Rabb, Leonard: Heat-Shield Performance During Atmospheric Entry of Project Mercury Research and Development Vehicle. NASA TM X-490, 1961.
3. Brown, Steve W., and Moseley, William C., Jr.: Summary of Wind-Tunnel Investigations of the Static Longitudinal Stability Characteristics of the Production Mercury Configurations at Mach Numbers From 0.05 to 20. NASA TM X-491, 1961.
4. Minzner, R. A., Champion, K. S. W., and Pond, H. L.: The ARDC Model Atmosphere, 1959. Air Force Surveys in Geophysics No. 115 (AFCRC-TR-59-267), Air Force Cambridge Res. Center, Aug. 1959.
5. Pritts, O. R., and Mallard, S. R.: Pressure and Heat Transfer Distribution on a One-Tenth Scale Mercury Capsule at Mach Number 8. AEDC-TN-59-164 (Contract No. AF 40(600)-800), Arnold Eng. Dev. Center, Jan. 1960.
6. Chapman, Dean R.: A Theoretical Analysis of Heat Transfer in Regions of Separated Flow. NACA TN 3792, 1956.
7. Eckert, E. R. G.: Engineering Relations for Friction and Heat Transfer to Surfaces in High Velocity Flow. Jour. Aero. Sci., (Readers' Forum), vol. 22, no. 8, Aug. 1955, pp. 585-587.
8. Weston, Kenneth C., and Swanson, Joanna E.: A Compilation of Wind-Tunnel Heat-Transfer Measurements on the Afterbody of the Project Mercury Capsule Reentry Configuration. NASA TM X-495, 1961.

DECLASSIFIED

13

TABLE I.- AFTERBODY INSTRUMENTATION

[All thermocouples were chromel-alumel.]

Thermocouple	Material	Wall thickness, in.	Wetted distance from shoulder, in.	Station in.
1	Inconel	0.0625	7.78	7.31
2	Inconel	0.0625	11.78	11.08
3	Inconel	0.0625	15.78	14.81
4	Inconel	0.0625	19.78	18.60
5	Inconel	0.0625	23.78	22.30
6	Inconel	0.050	31.78	29.92
7	Inconel	0.050	39.78	37.30
8	Inconel	0.050	47.78	45.00
9	Inconel	0.050	55.78	52.50
10	Inconel	0.050	63.08	59.40
11	Inconel	0.03125	67.04	63.14
12	Inconel	0.03125	74.04	70.14
13	Inconel	0.03125	81.04	77.14
14	Inconel	0.03125	90.04	86.12
15	Inconel	0.03125	104.04	100.07
16	Fiber glass	0.125	109.04 (9-inch radius on pitch plane)	105.14
17	Inconel	0.03125	97.04	93.07
18	Inconel	0.03125	77.54	73.14
19	Inconel	0.03125	70.54	66.14
20	Inconel	0.050	55.78	52.50
21	Inconel	0.0625	23.78	22.30
22	Inconel	0.0625	15.78	14.81
23	Inconel	0.0625	7.78	7.31
24	Inconel	0.0625	15.78	14.81
28	Inconel	0.050	47.78	45.00

031712281030

14

TABLE I.- AFTERBODY INSTRUMENTATION - Concluded.

[All thermocouples were chromel-alumel.]

Thermocouple	Material	Wall thickness, in.	Wetted distance from shoulder, in.	Station in.
29	Inconel	0.03125	74.04	70.14
30	Inconel	0.03125	97.04	93.07
34	Inconel	0.0625	15.78	14.81
35	Inconel	0.0625	15.78	14.81
36	Inconel	0.0625	15.78	14.81
42	Inconel	0.0625	23.78	22.30
43	Inconel	0.0625	19.78	18.60
44	Inconel	0.0625	11.78	11.08
45	Inconel	0.0625	7.78	7.31
47	Inconel	0.050	62.08	58.40
48	Inconel	0.050	37.78	35.60
49	Inconel	0.050	47.78	45.00
50	Inconel	0.050	47.78	45.00
51	Inconel	0.050	47.78	45.00
52	Inconel	0.050	47.78	45.00
53	Fiber glass	0.125	109.04 (9-inch radius, 60° from pitch plane)	105.14

UNCLASSIFIED

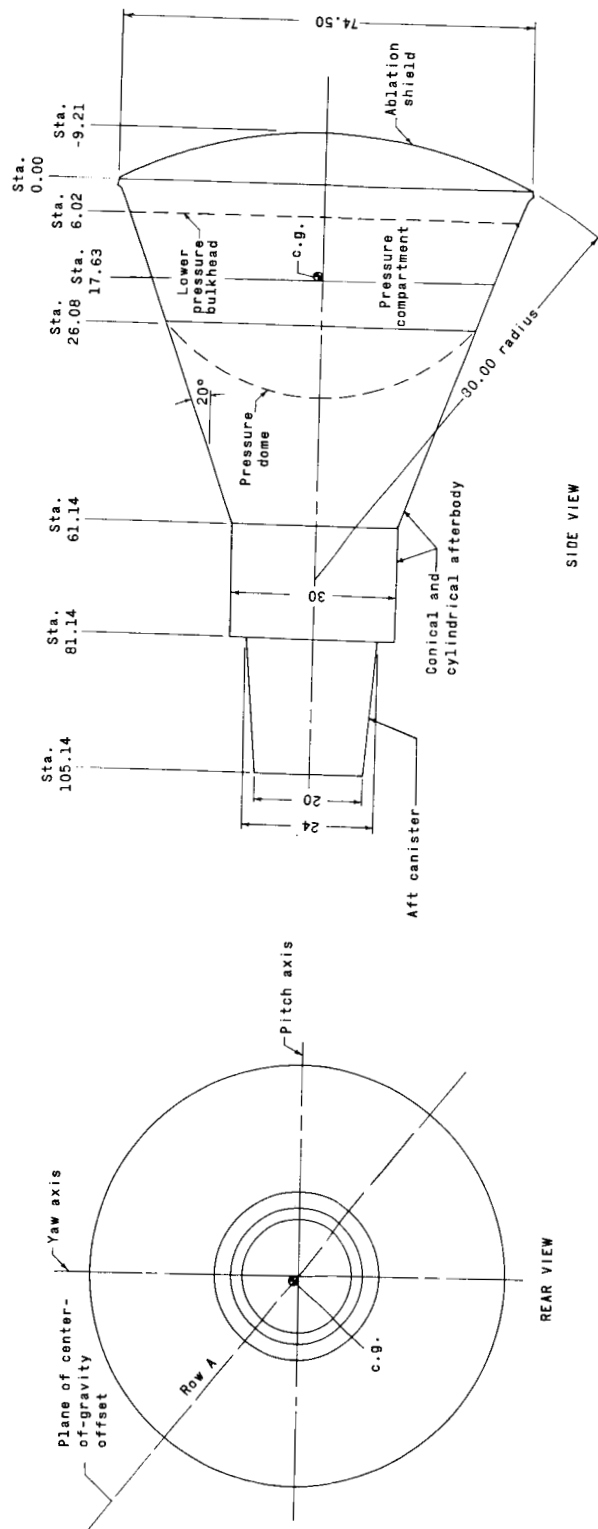


Figure 1.- Sketch of capsule. Dimensions are in inches. Center-of-gravity offset is not to scale.

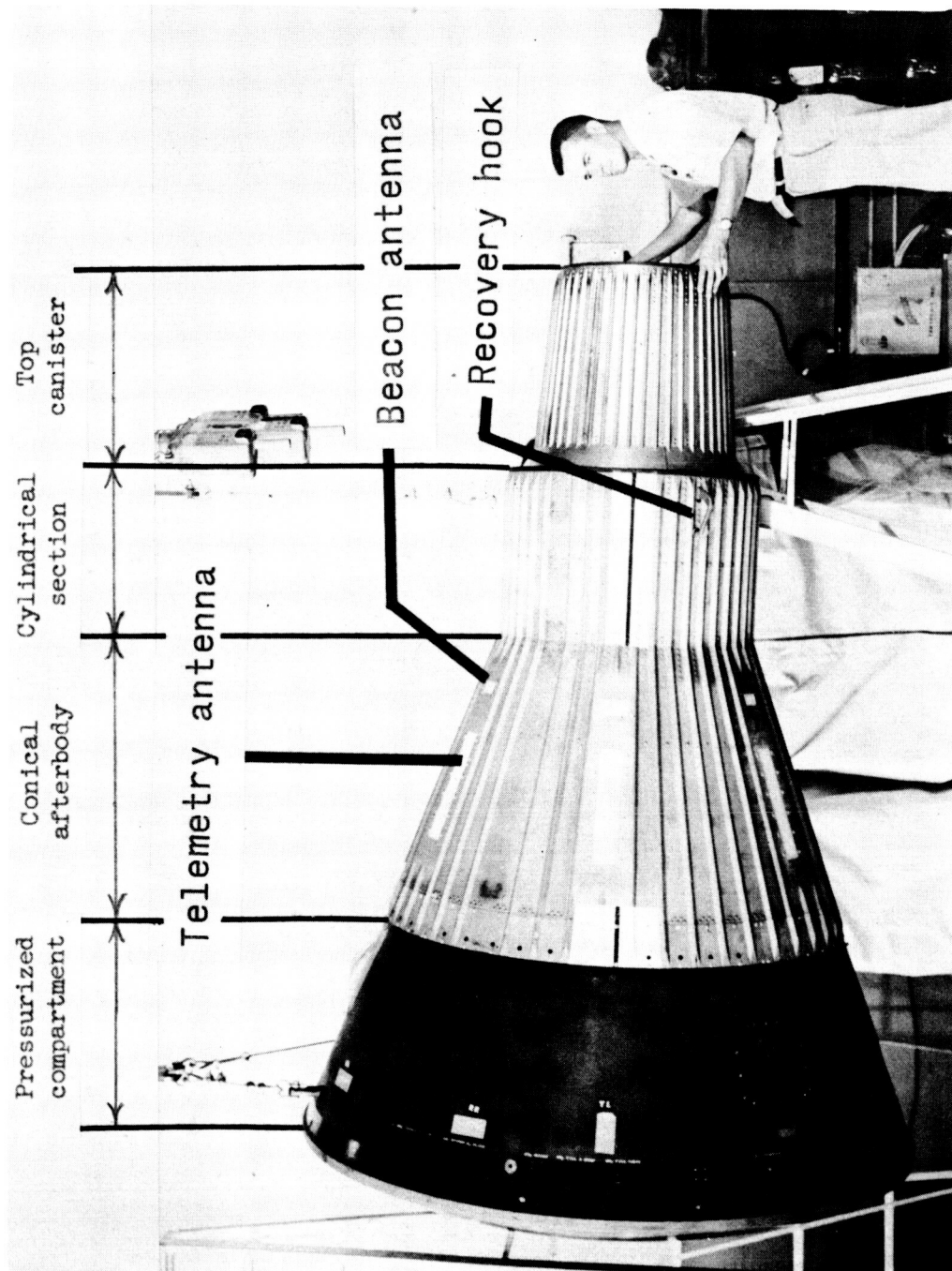


Figure 2.- Assembled capsule.

G-60-2101.1

DATA ACQUIRED

G
5

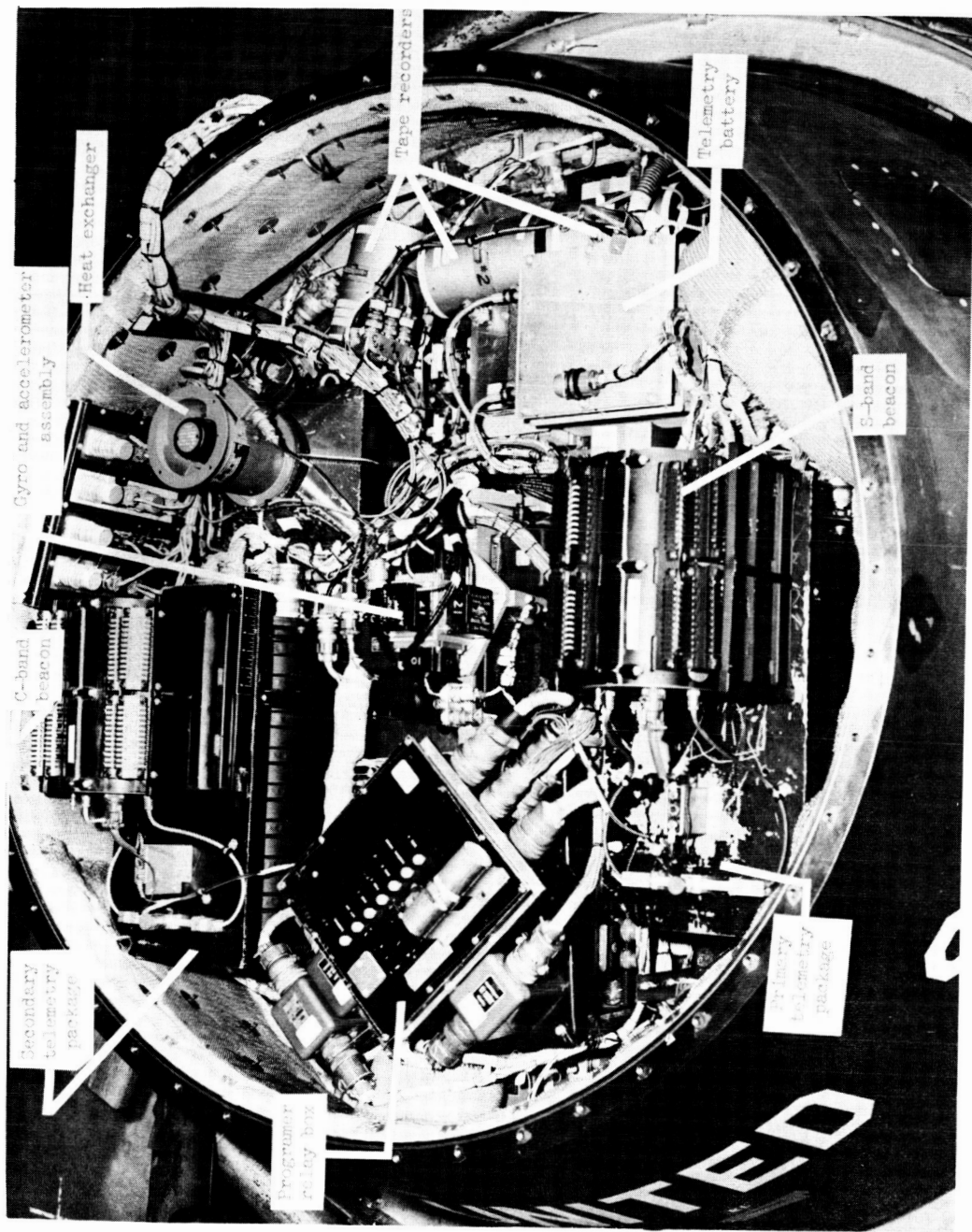
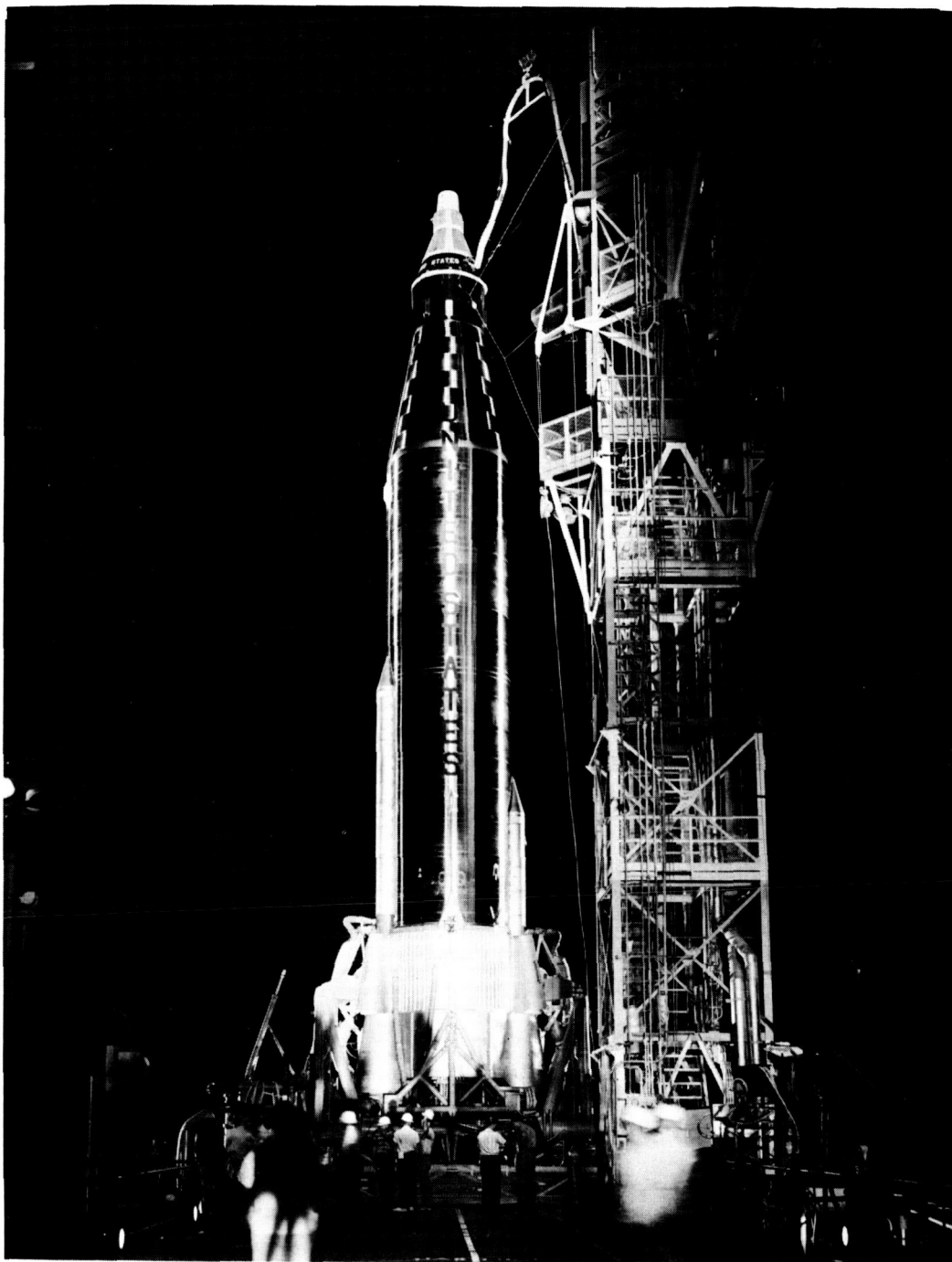


Figure 3.- Arrangement of instrumentation in pressurized compartment. G-60-2104.1



G-60-2105

Figure 4.- Capsule mounted on Atlas 10-D booster on launch stand.



Figure 5.- Sketch of afterbody thermocouple locations. The six thermocouples in A-A and B-B are equally spaced.

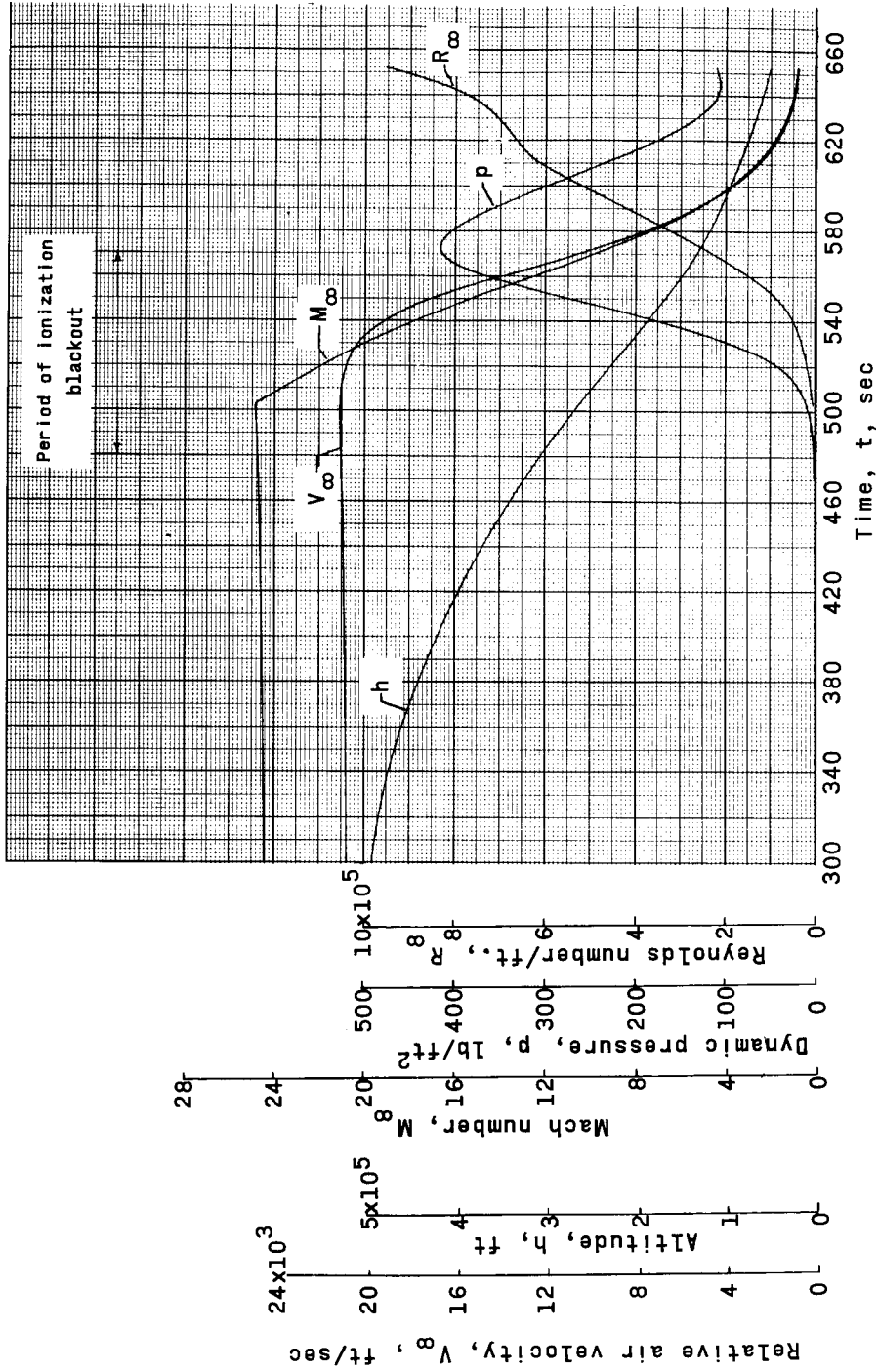


Figure 6.- Time history of Big Joe flight parameters.

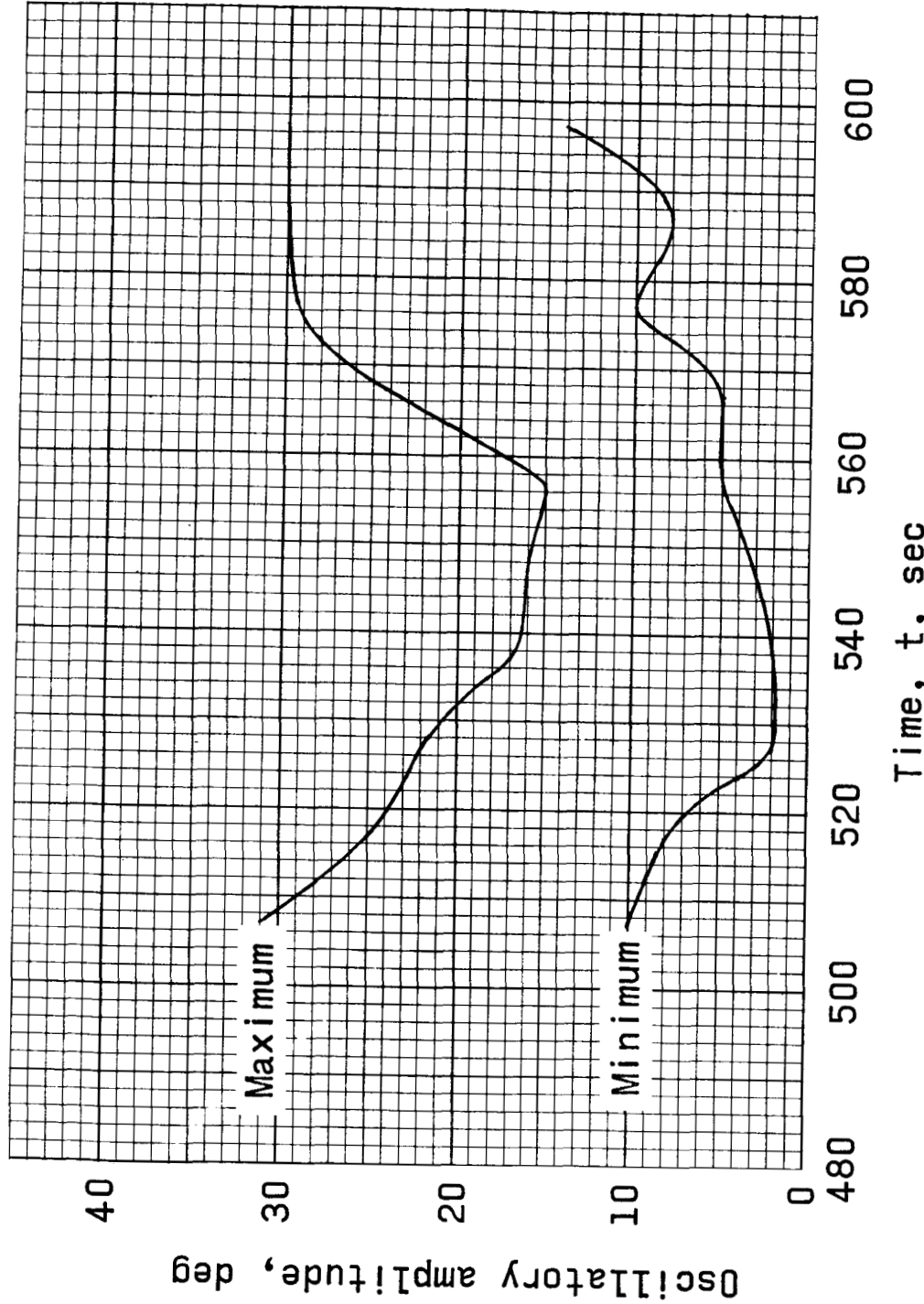


Figure 7.- Oscillatory amplitude about trim as a function of time.

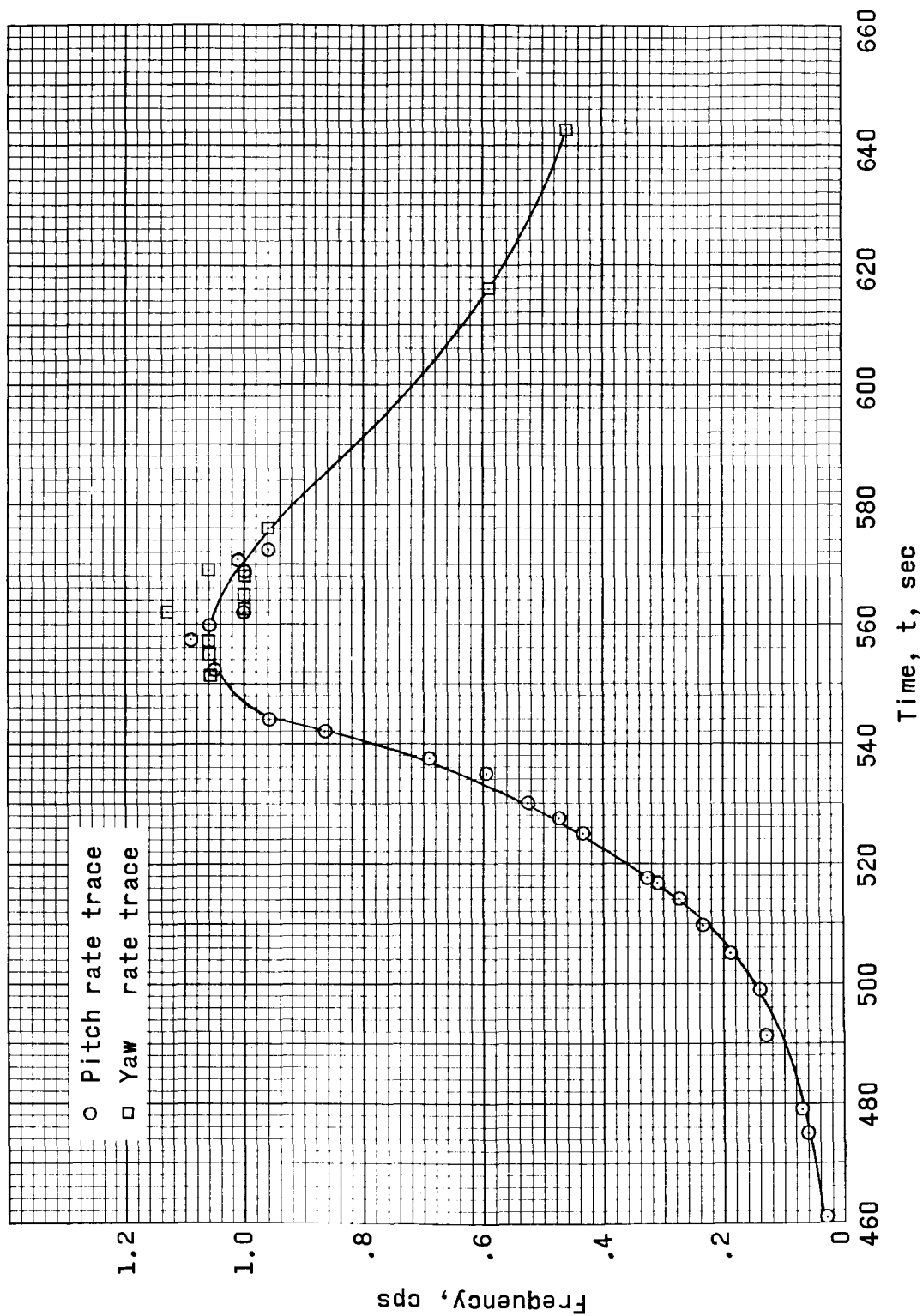
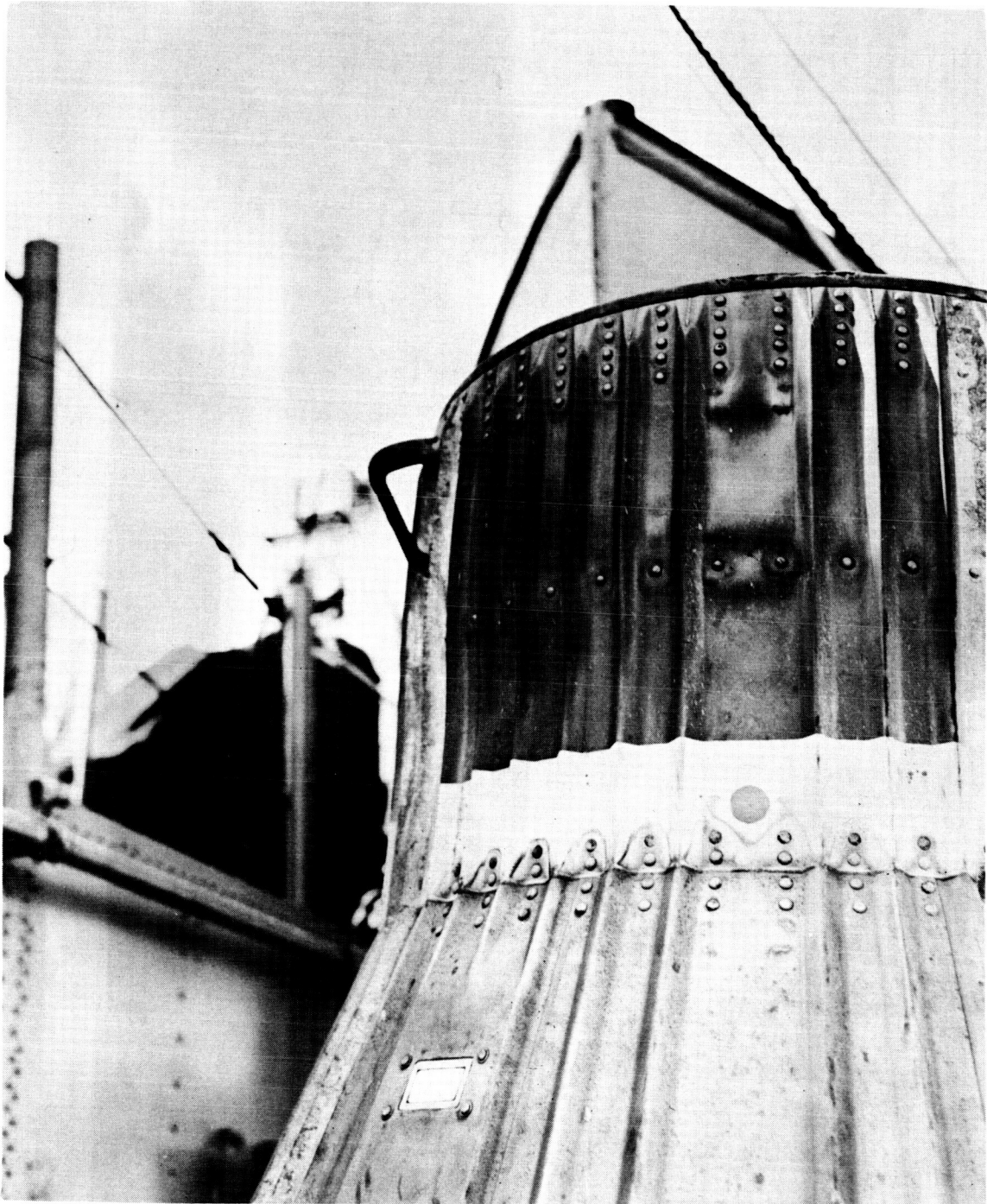


Figure 8.- Frequency of oscillation from pitch and yaw rate as a function of time.

DECLASSIFIED

23



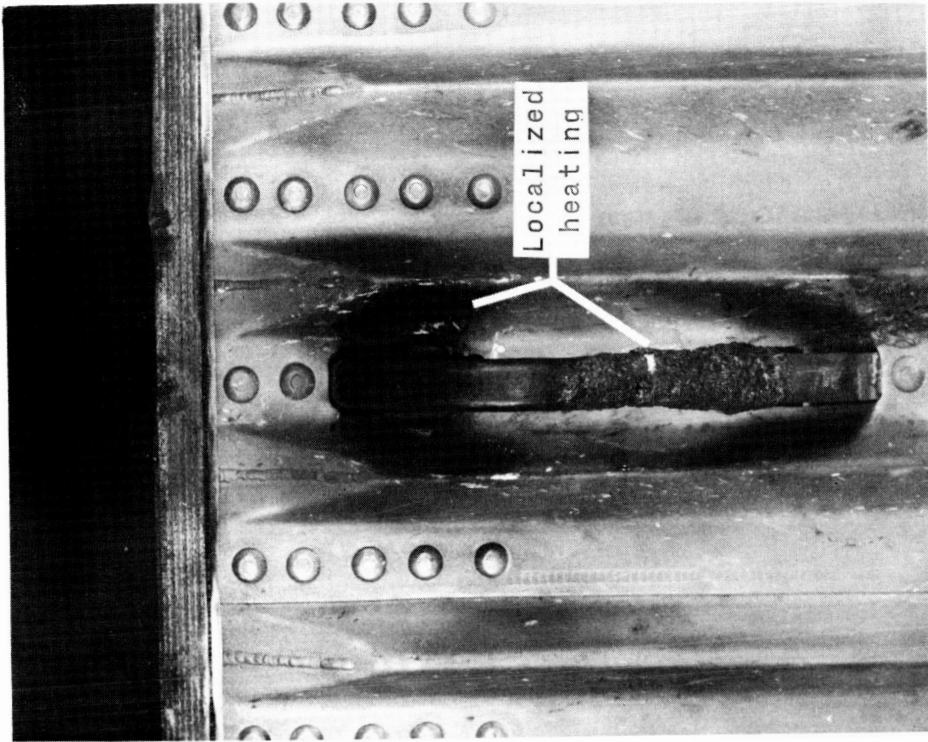
(a) Skin buckling on cylinder.

G-61-7

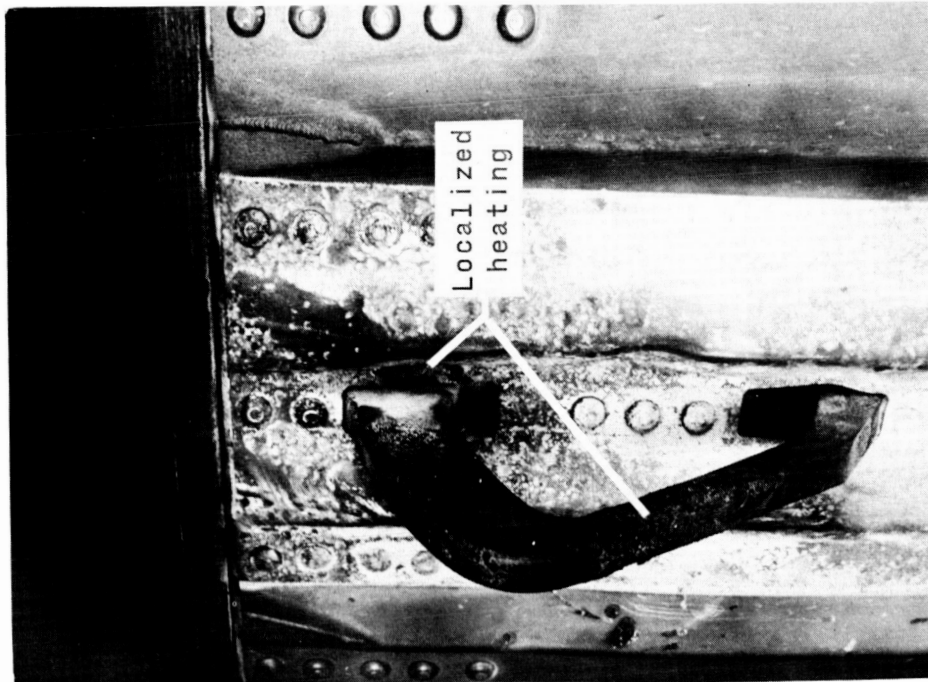
Figure 9.- Results of localized heating.

03171230.1330

24

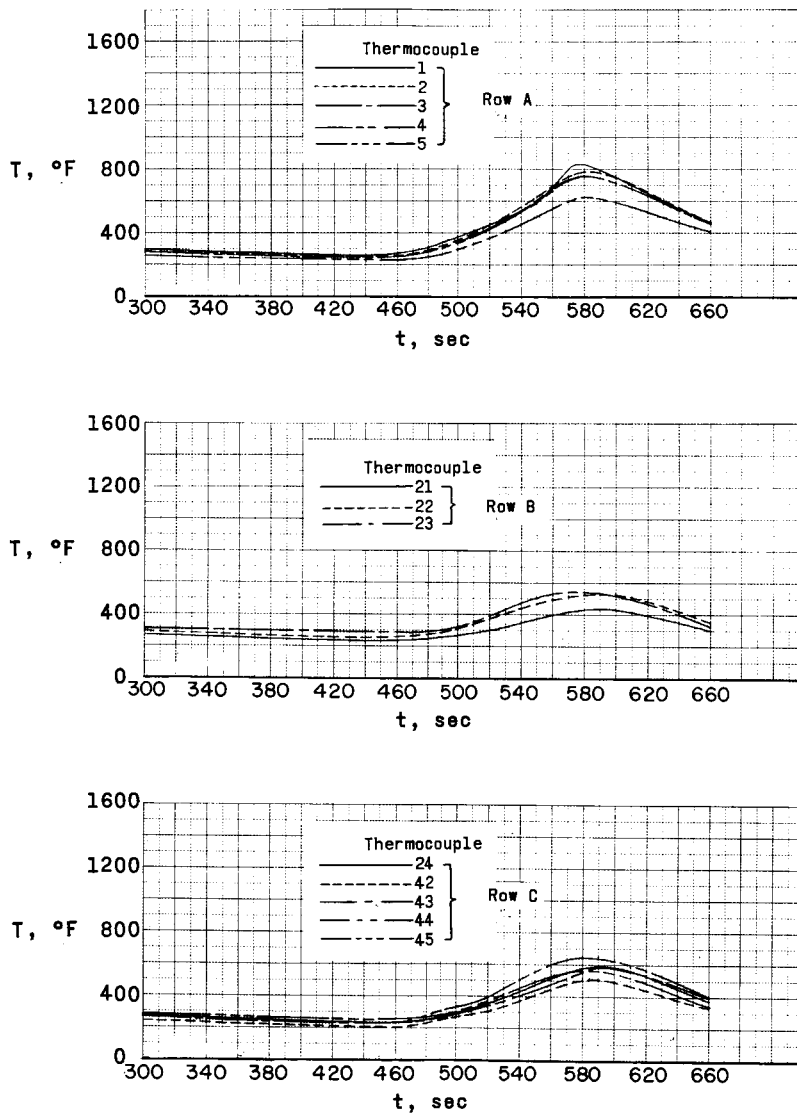


B-59-532.1
(c) Hook located in quadrant II.



B-59-528.1
(b) Hook located in pitch plane.

Figure 9. - Concluded.

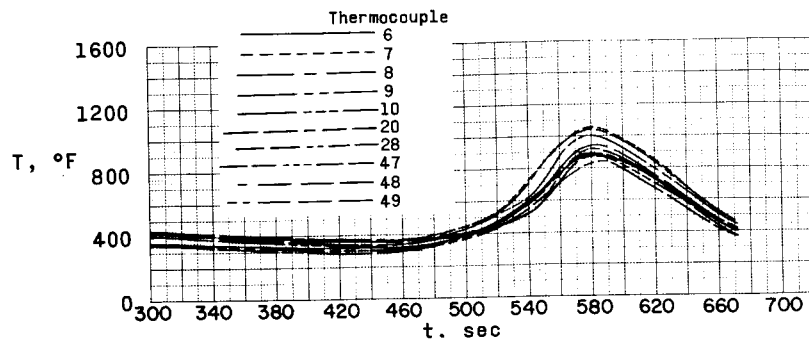


(a) Pressure vessel sidewalls.

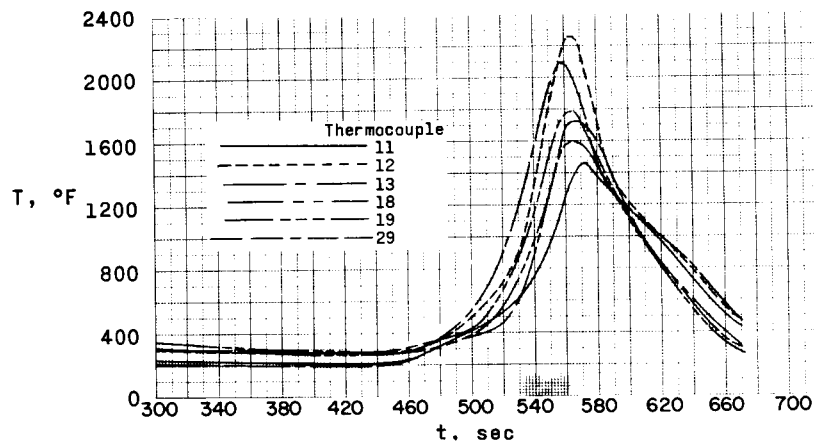
Figure 10.- Afterbody temperatures during reentry heating.

03/10/2010

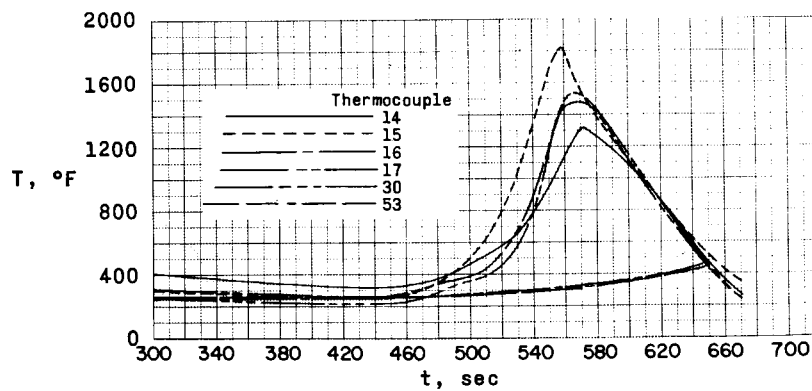
26



(b) Cone sidewall.



(c) Cylinder.

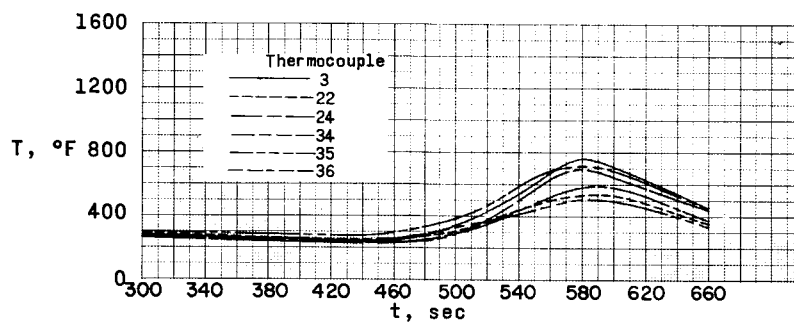


(d) Top canister.

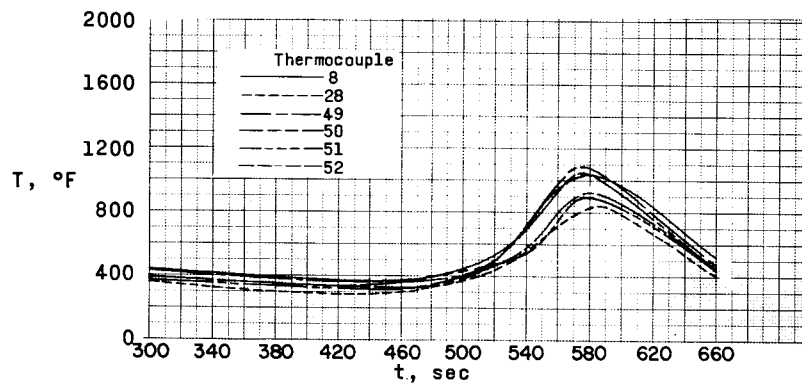
Figure 10.- Continued.

DECLASSIFIED

27



(e) Section A-A.



(f) Section B-B.

Figure 10.- Concluded.

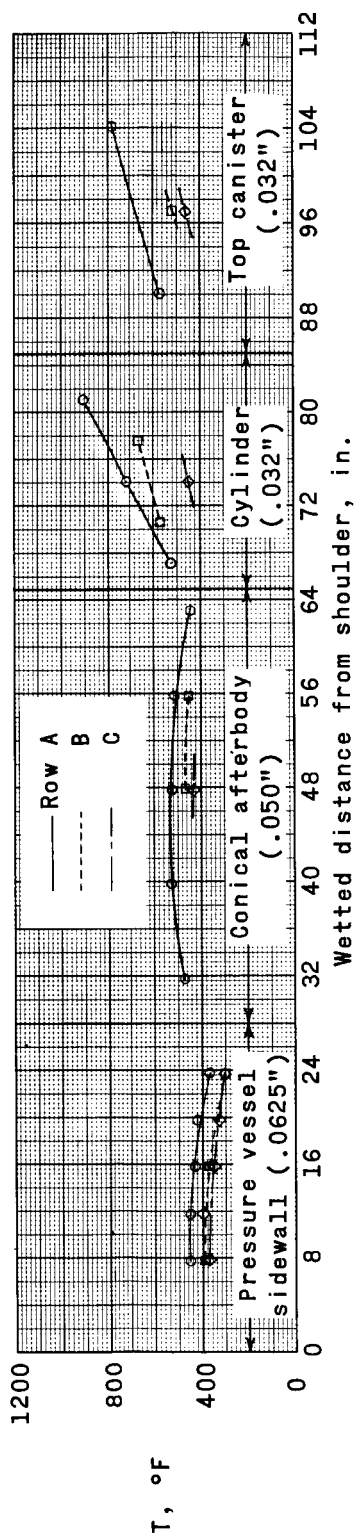
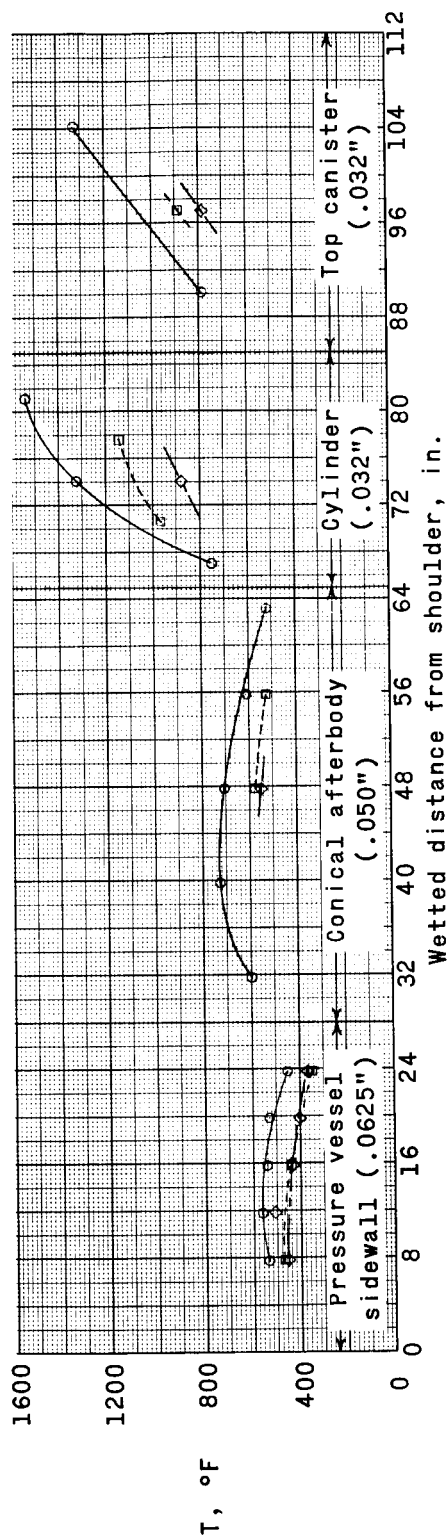
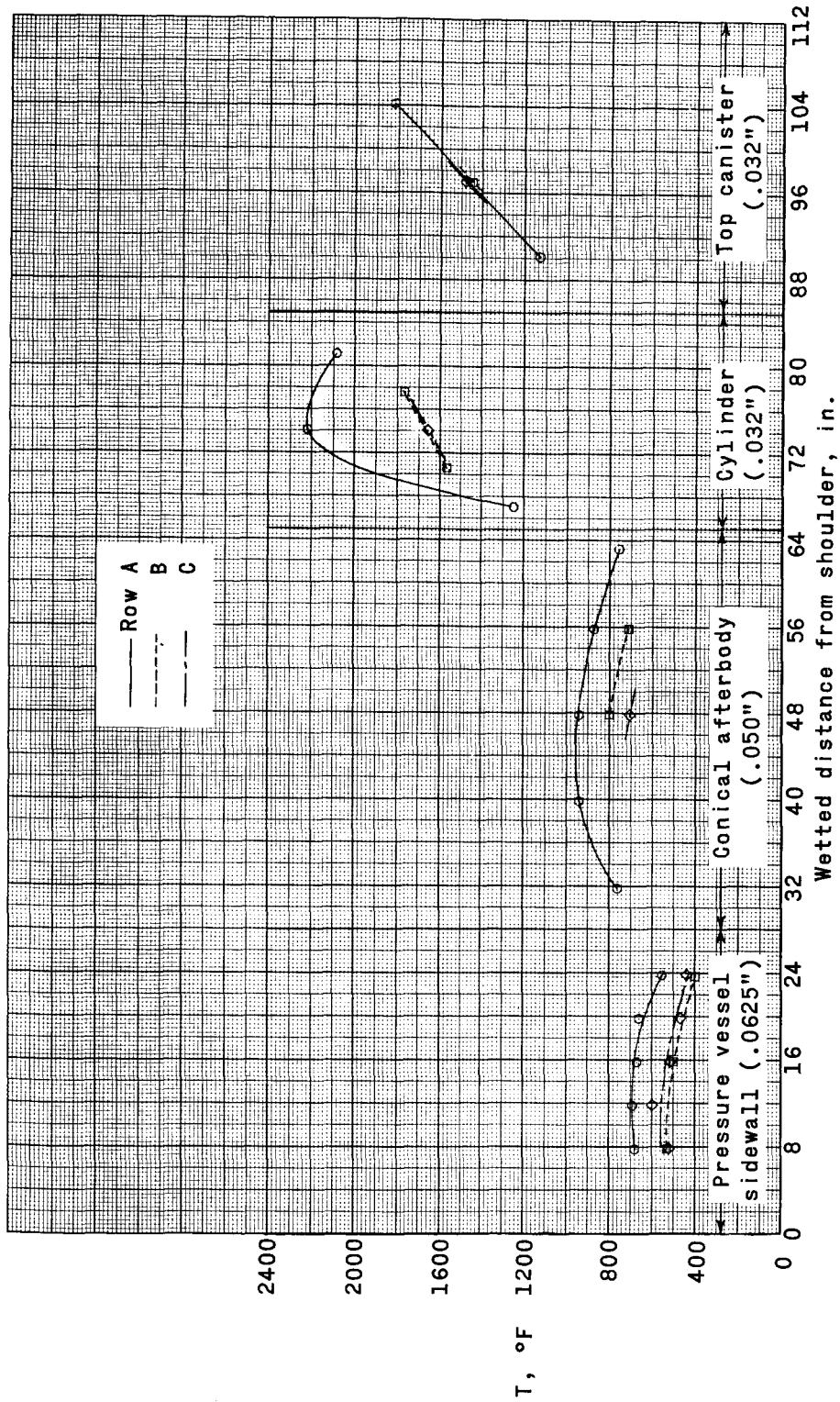
(a) $t = 520$ seconds.(b) $t = 540$ seconds.

Figure 11.- Temperature distribution along afterbody during reentry heating.

REF ID: A65718



(c) $t = 560$ seconds.

Figure 11.- Continued.

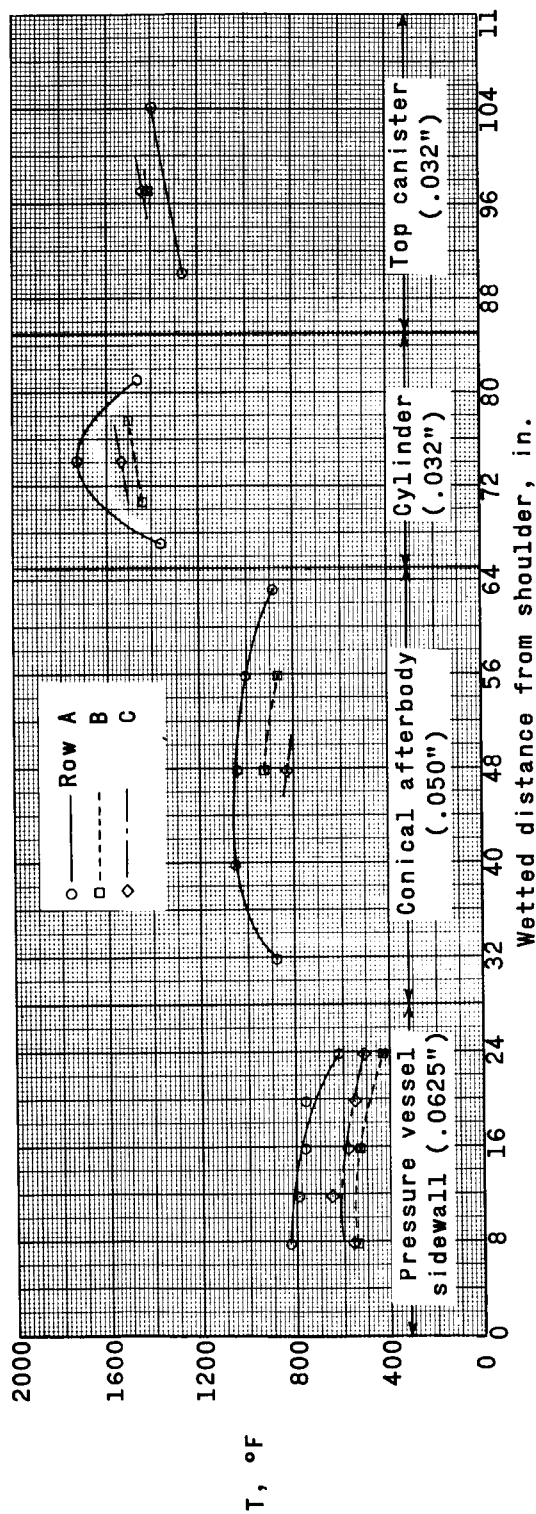
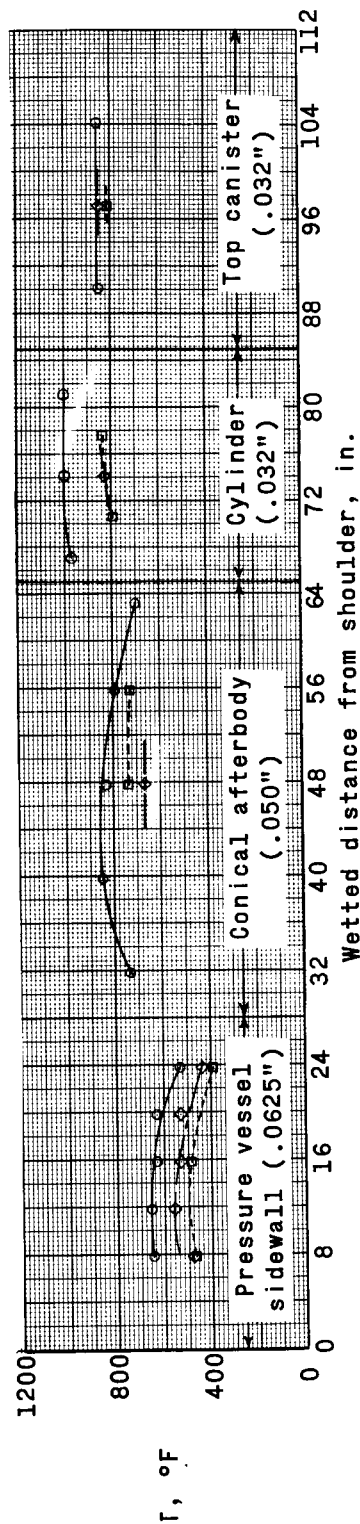
(d) $t = 580$ seconds.(e) $t = 620$ seconds.

Figure 11.- Concluded.

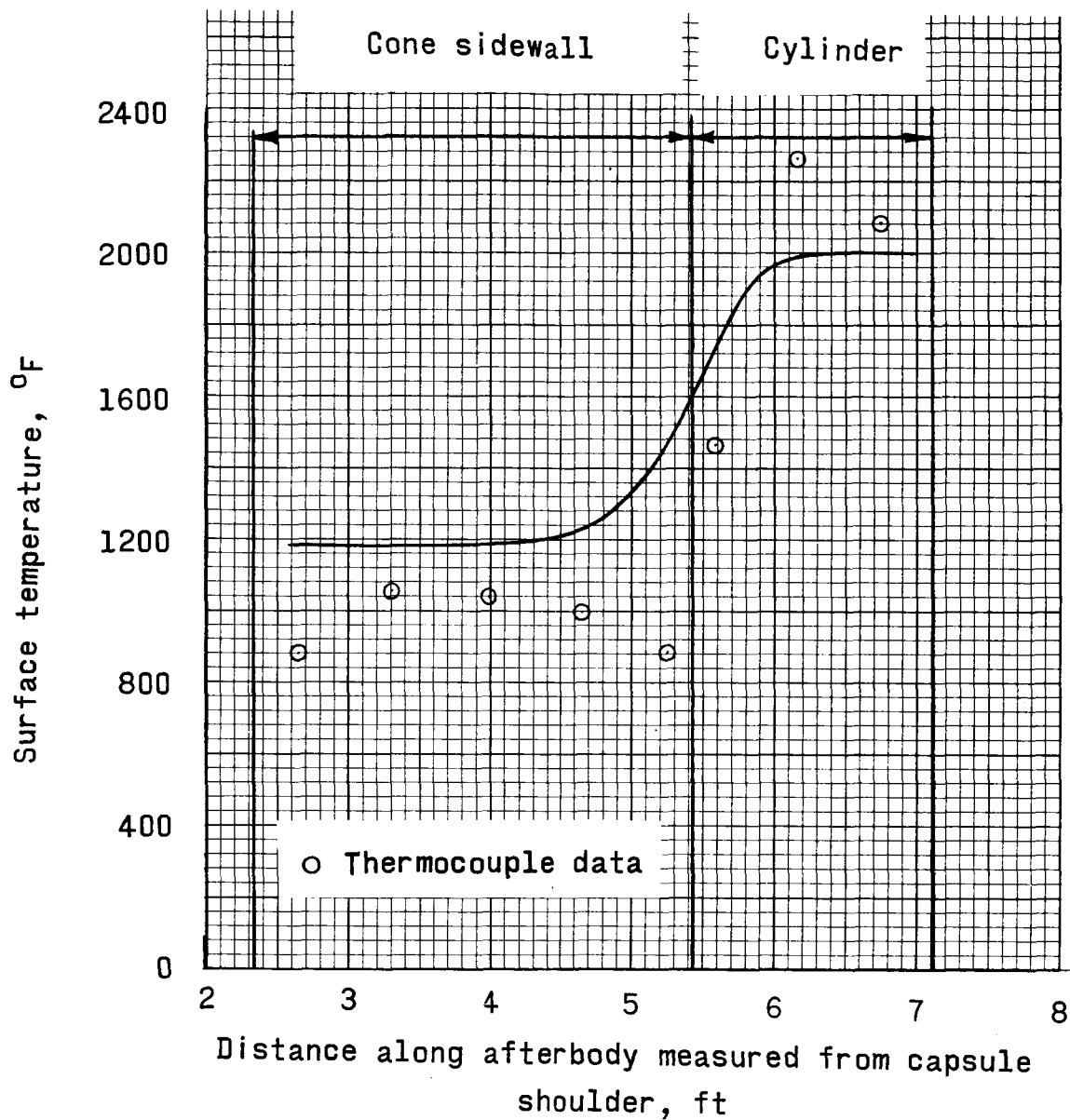
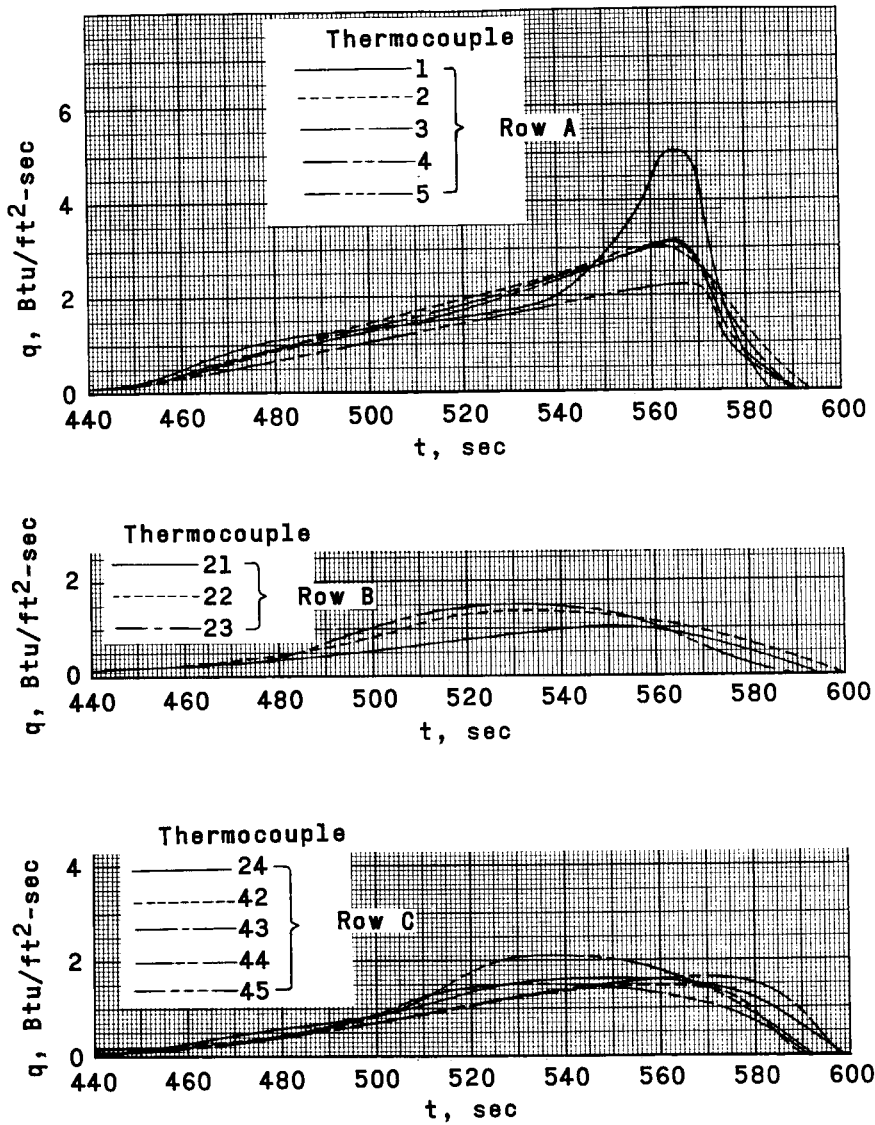
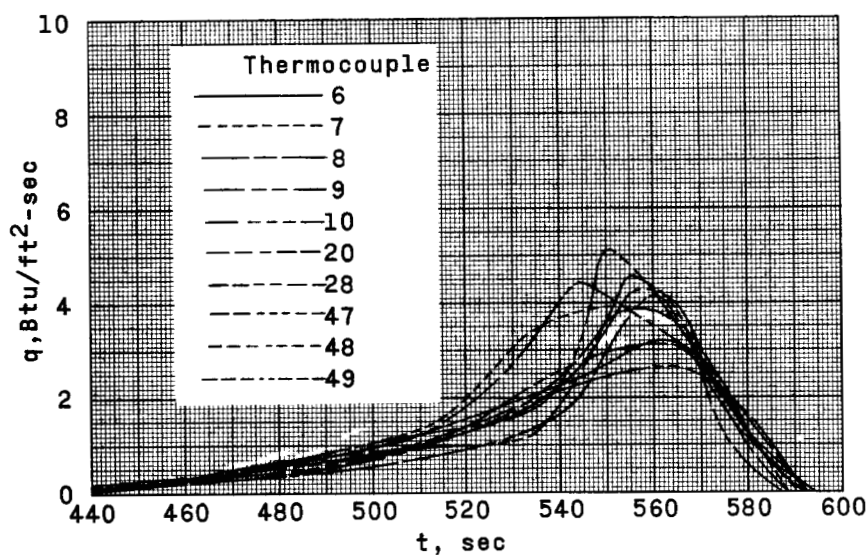


Figure 12.- Probable maximum temperature reached on afterbody as indicated by temperature-sensitive paint.



(a) Pressure vessel sidewall.

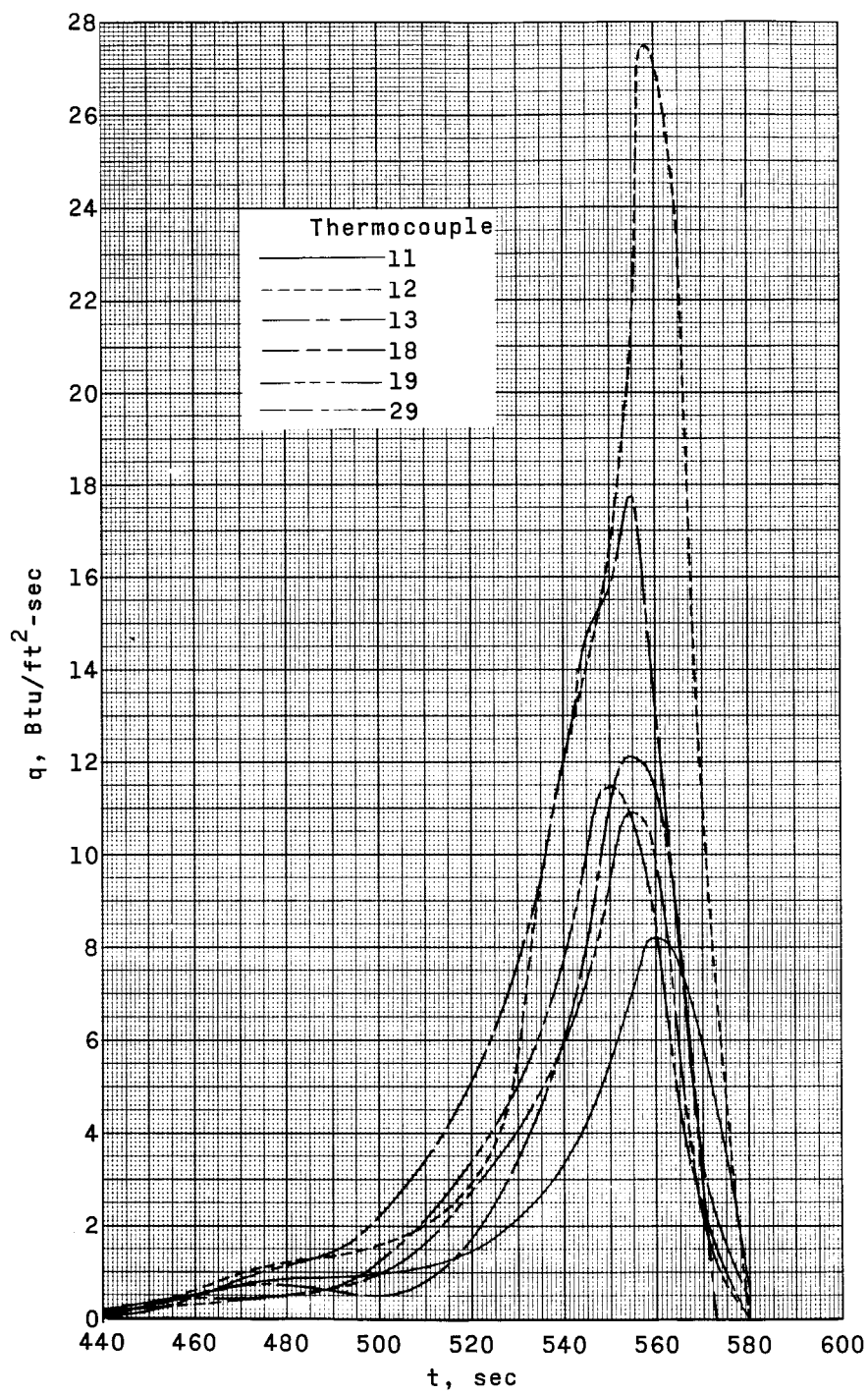
Figure 13.- Time histories of local heating rates during reentry.



(b) Cone sidewall.

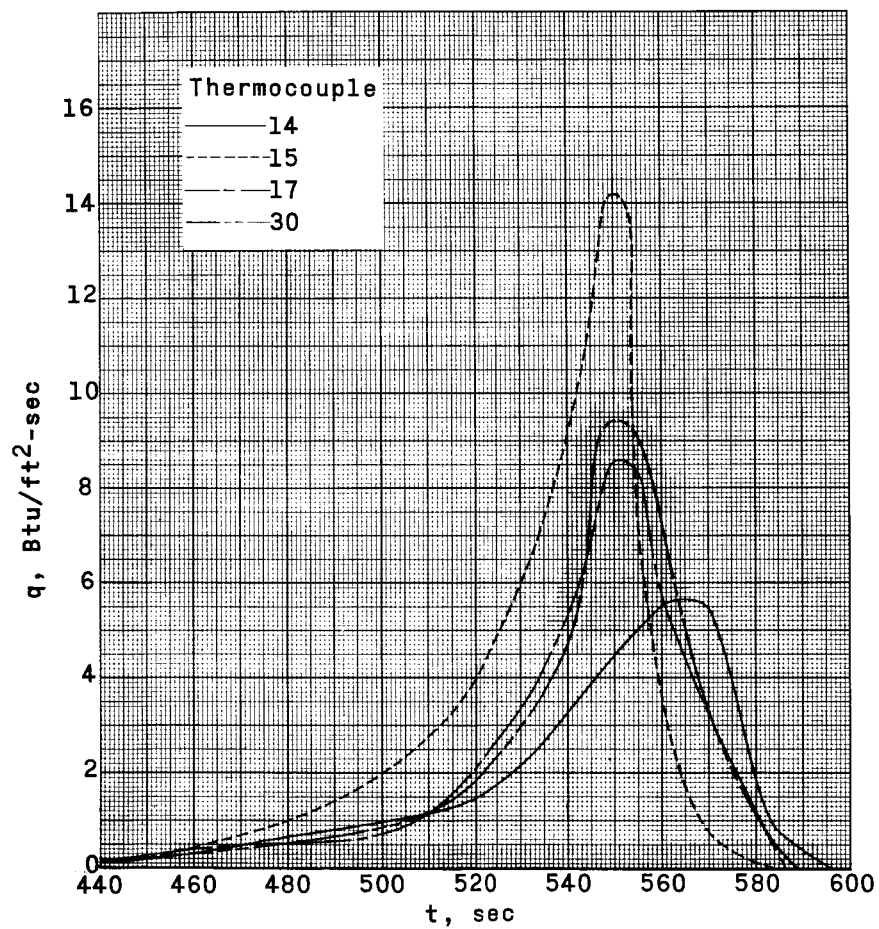
Figure 13.- Continued.

0371028 030



(c) Cylinder.

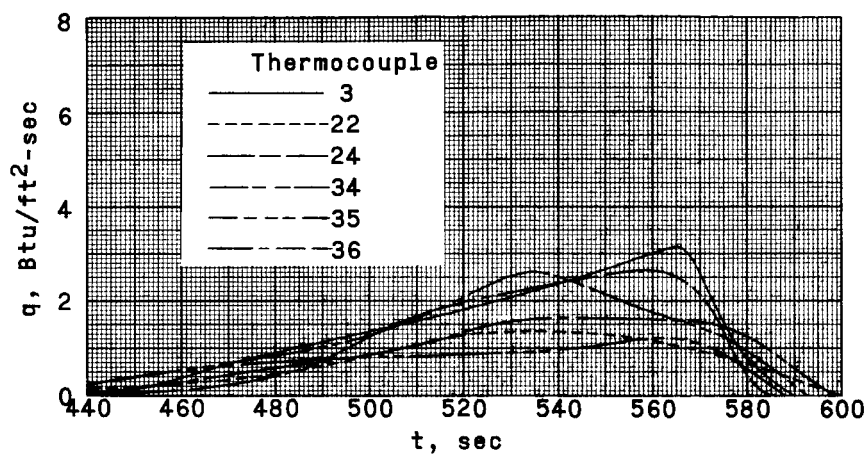
Figure 13.- Continued.



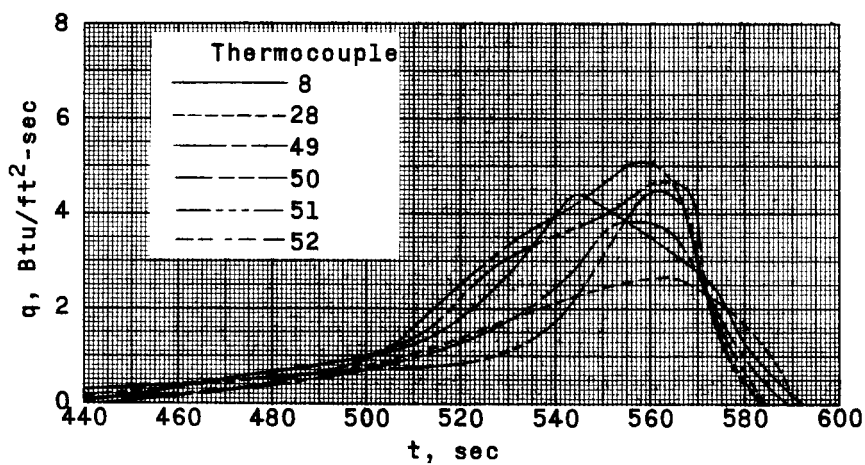
(d) Top canister.

Figure 13.- Continued.

031702A.1930



(e) Section A-A.



(f) Section B-B.

Figure 13.- Concluded.

DECLASSIFIED

37

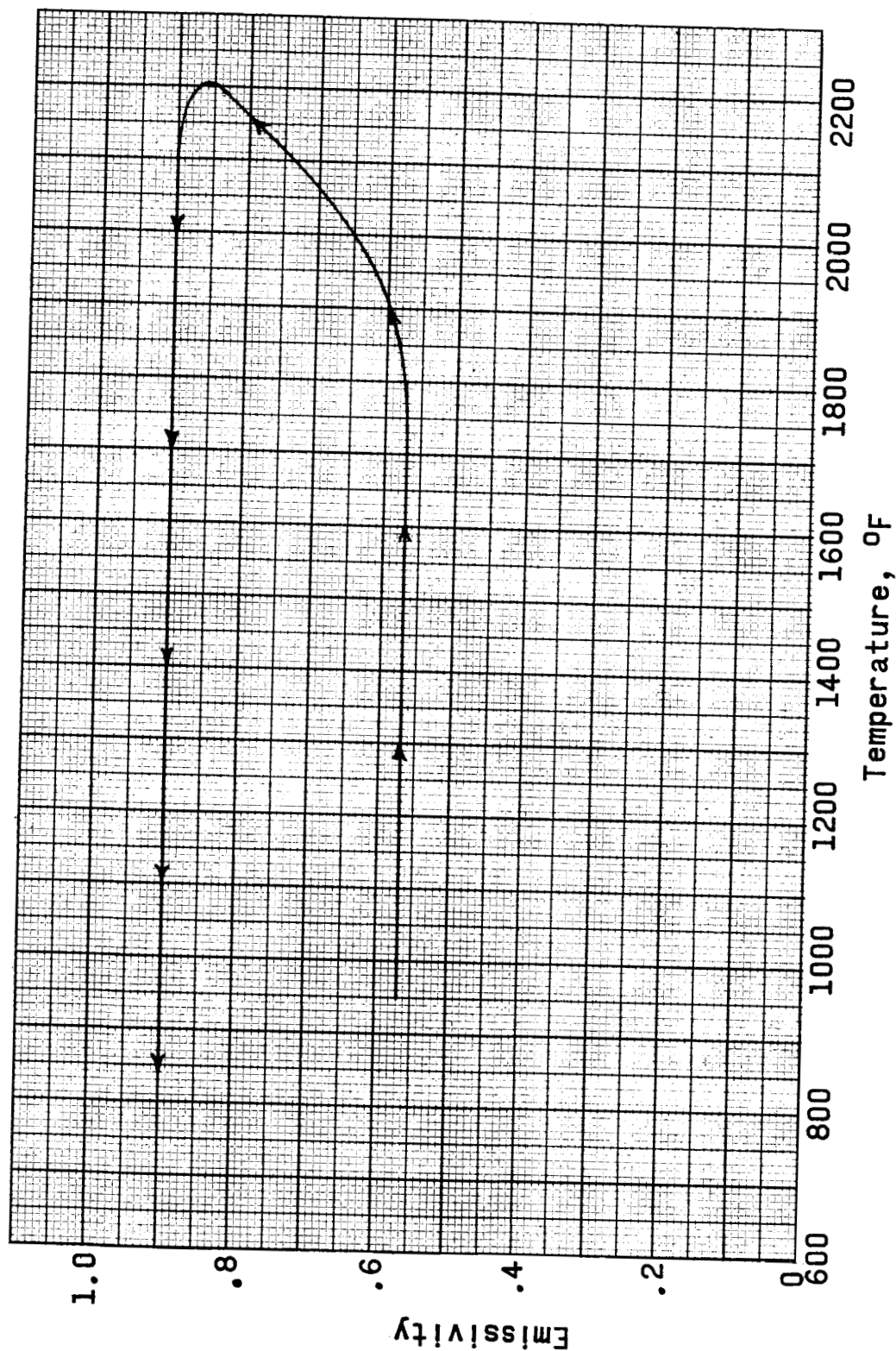
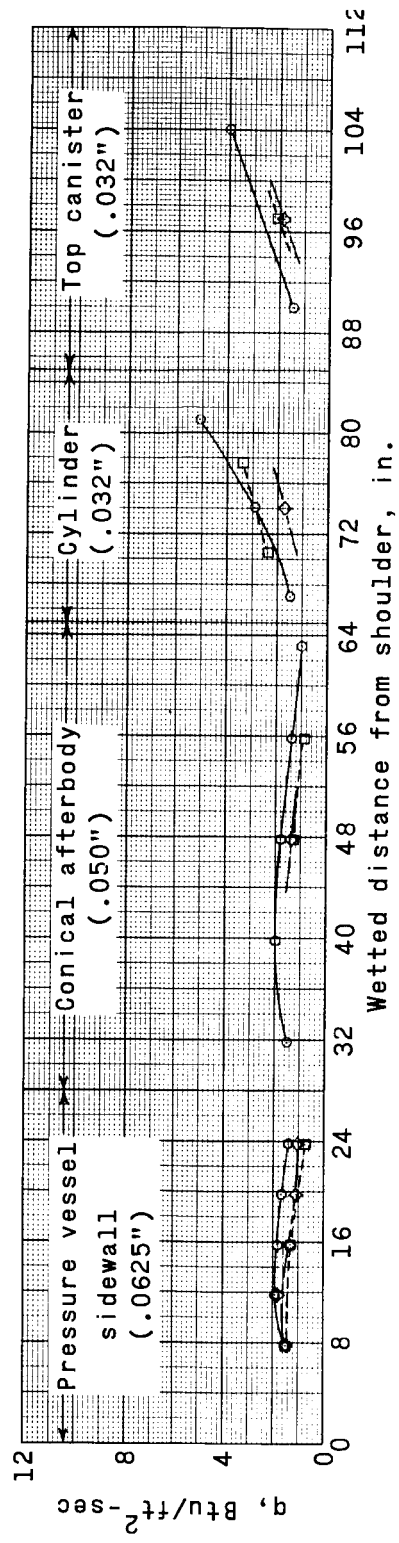
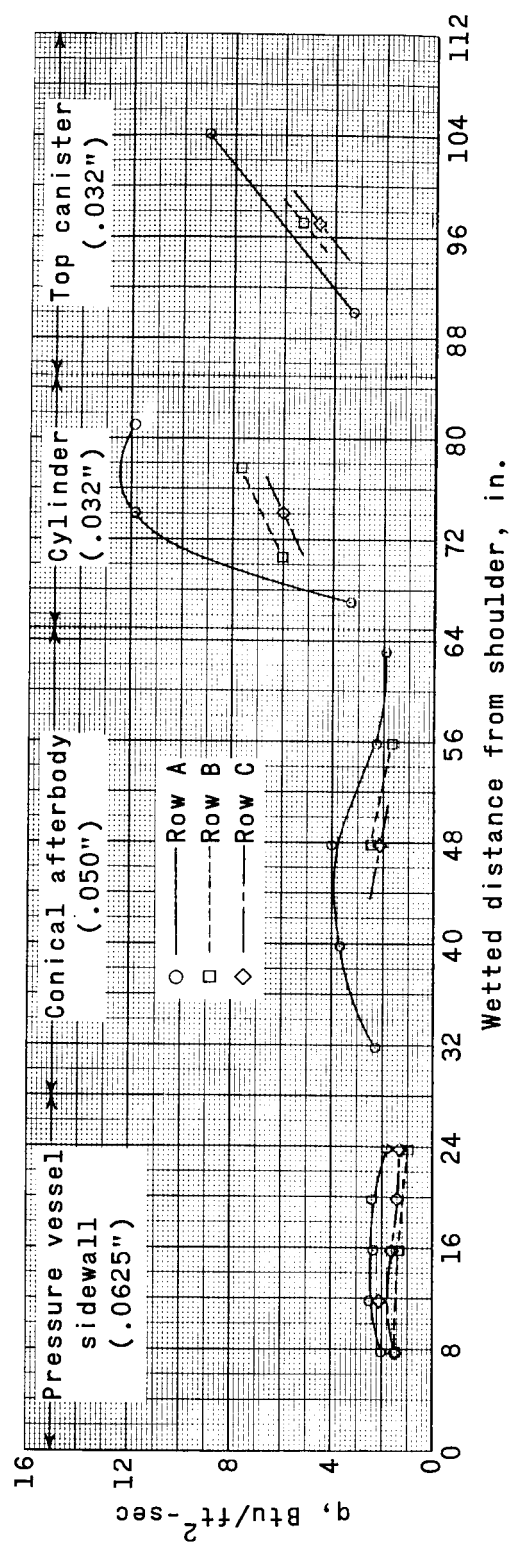


Figure 14.- Variation of the emissivity of Inconel with temperature as obtained in laboratory tests.

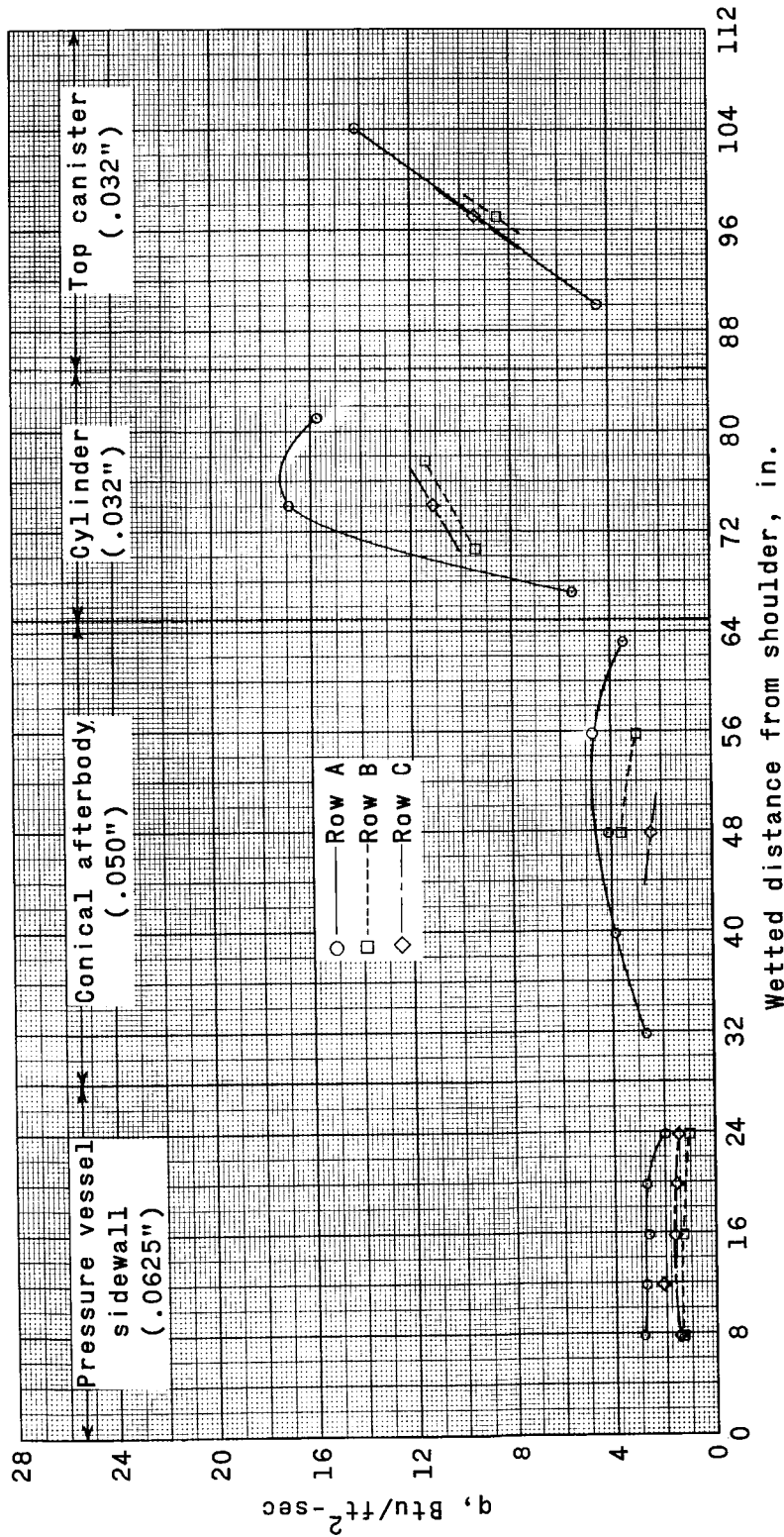


(a) $t = 520$ seconds.



(b) $t = 540$ seconds.

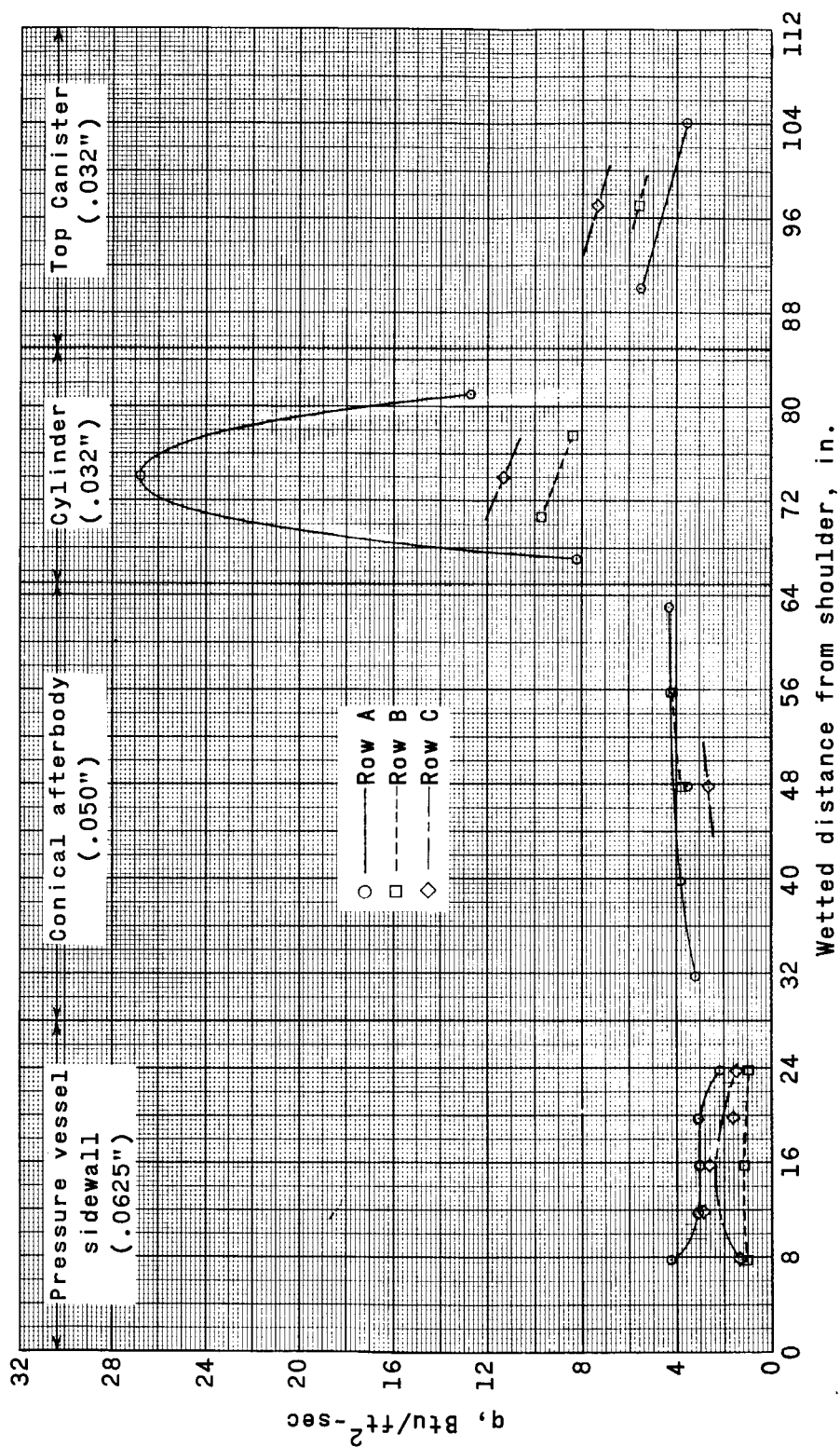
Figure 15.- Time histories of heating rates along afterbody during reentry.



(c) $t = 550$ seconds.

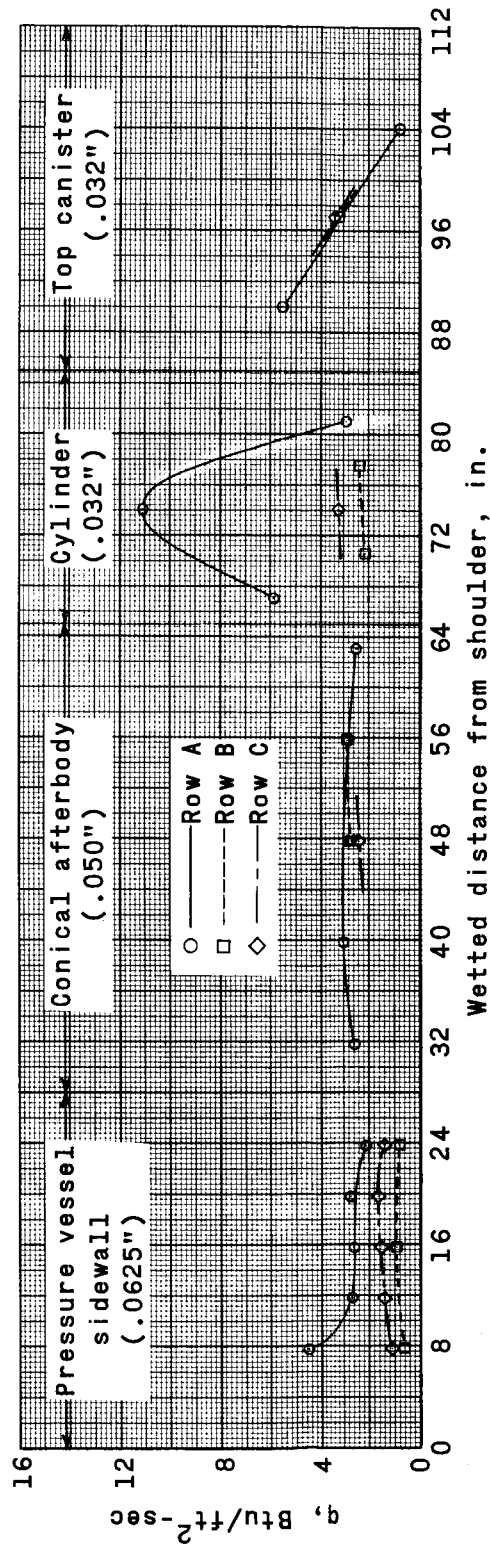
Figure 15.- Continued.

03:40:28.1530



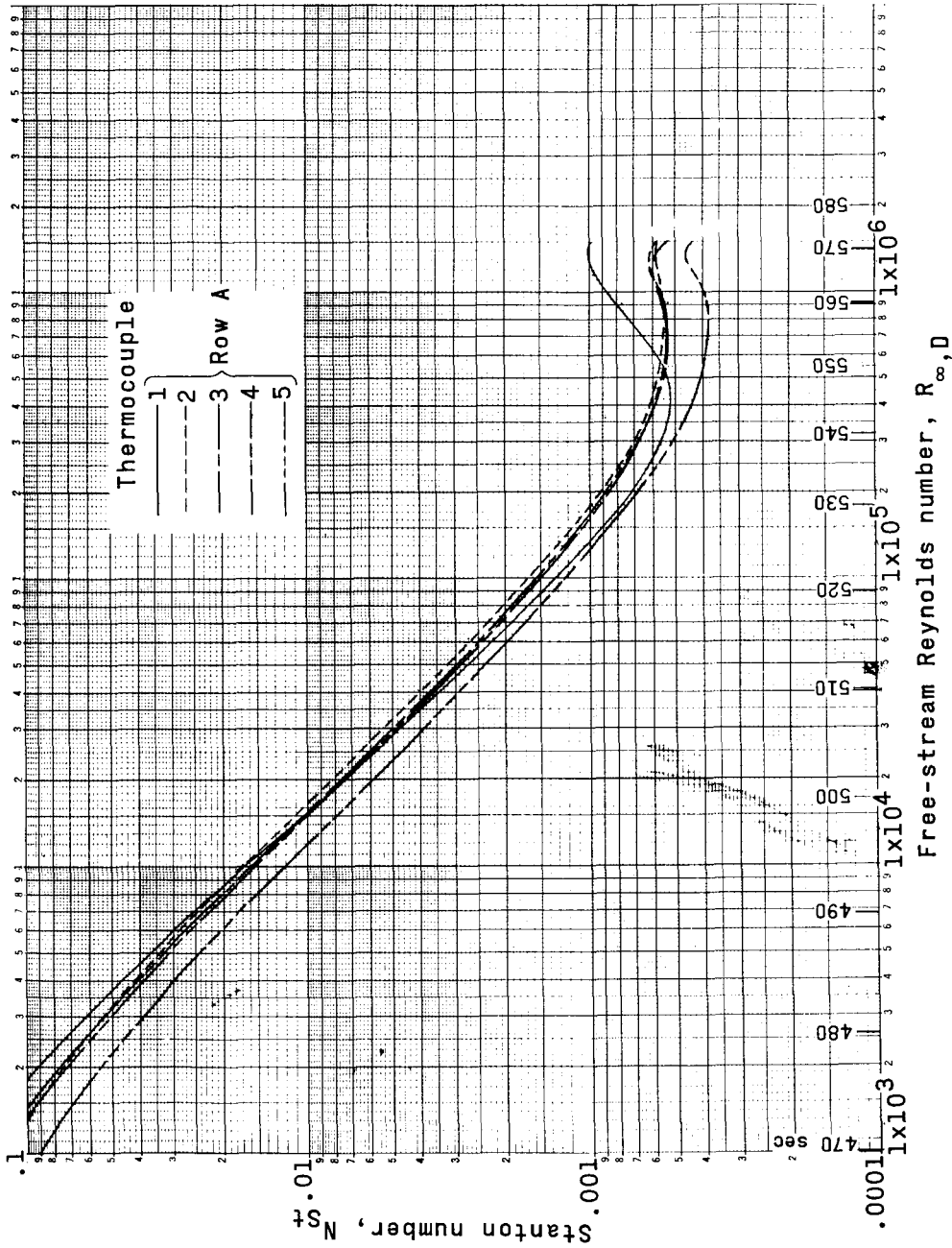
(d) $t = 560$ seconds.

Figure 15.- Continued.



(e) $t = 570$ seconds.

Figure 15.- Concluded.



(a) Pressure vessel sidewall.

Figure 16.- Variation of measured Stanton number with Reynolds number based on body diameter.

[REDACTED]

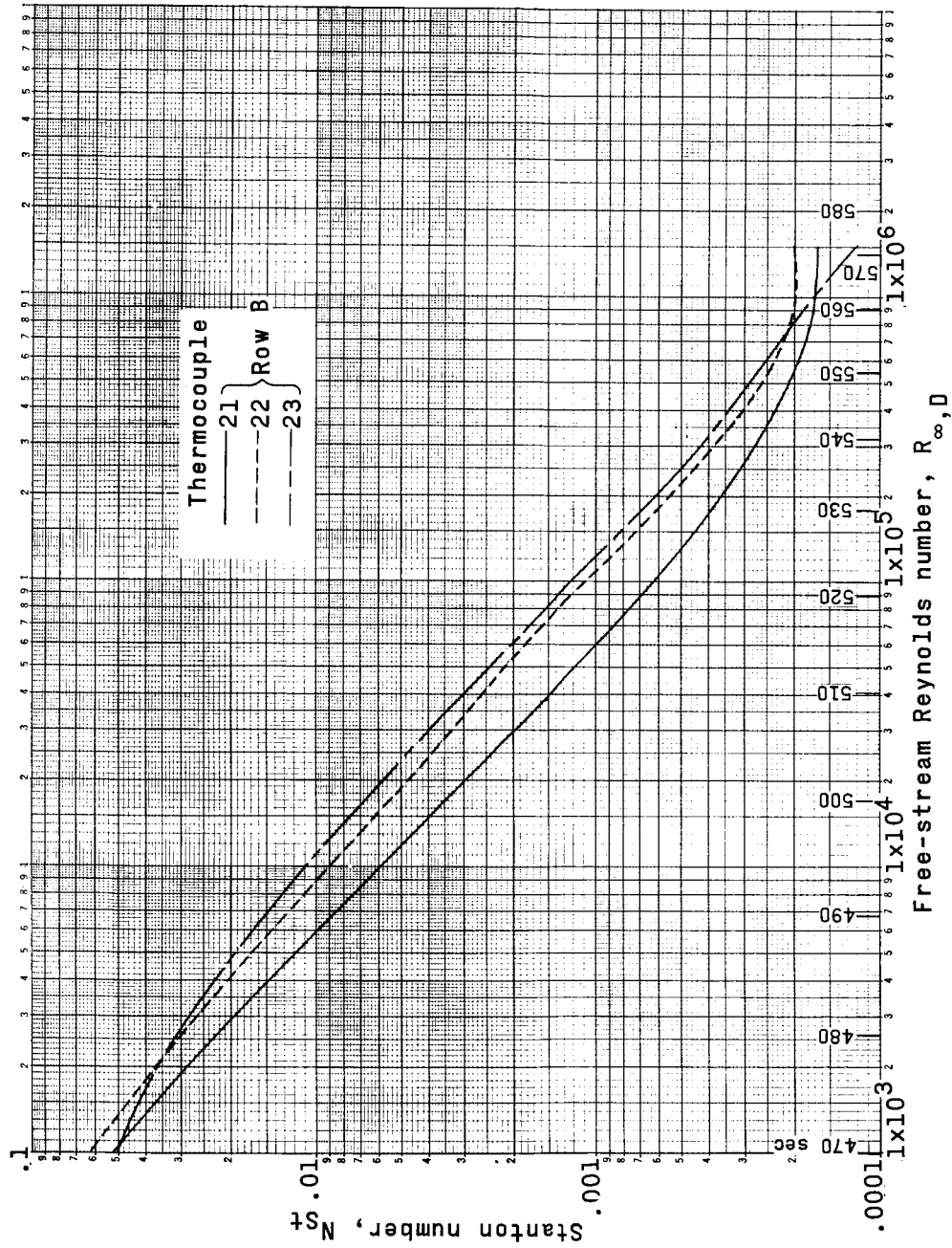
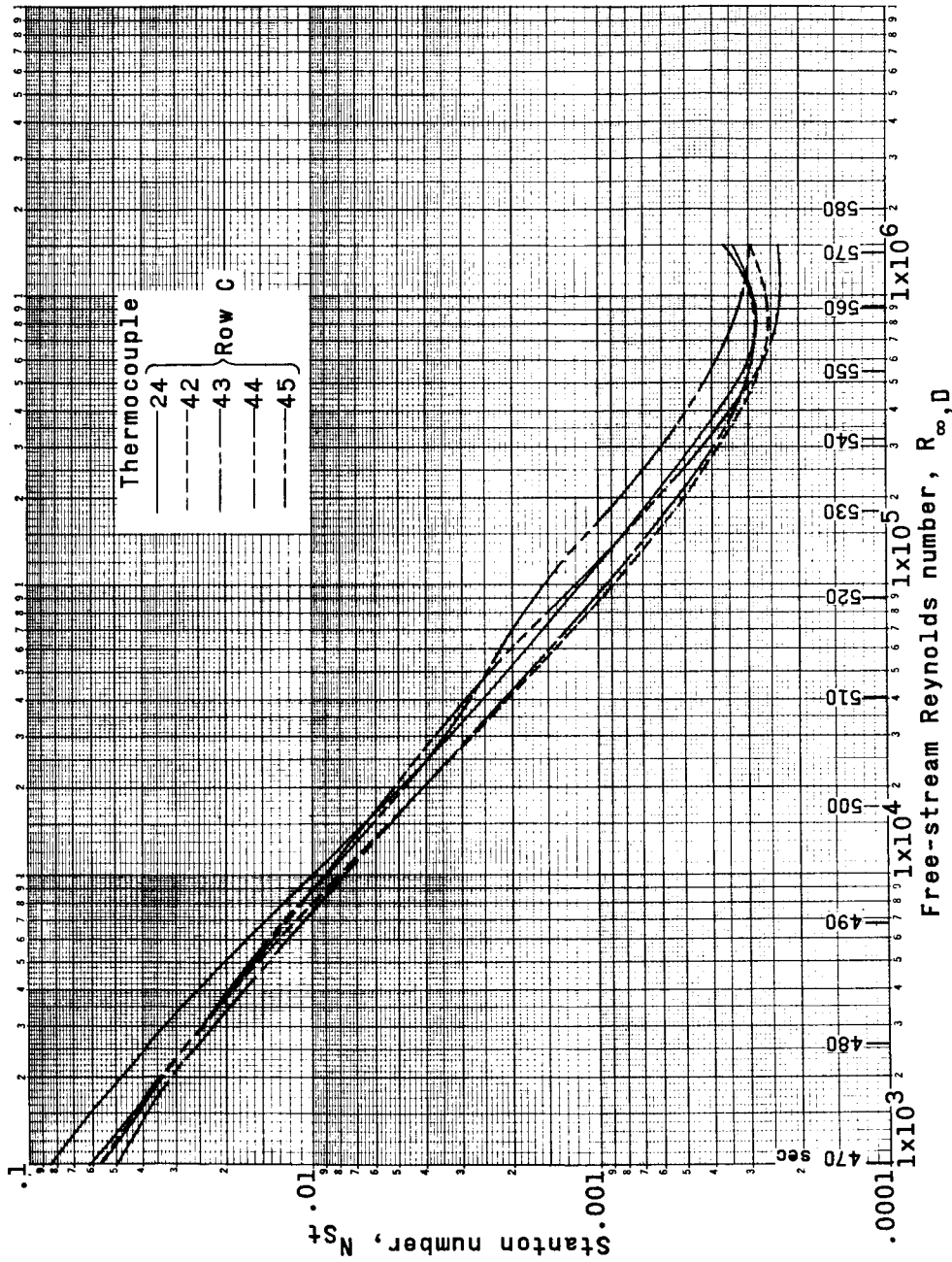
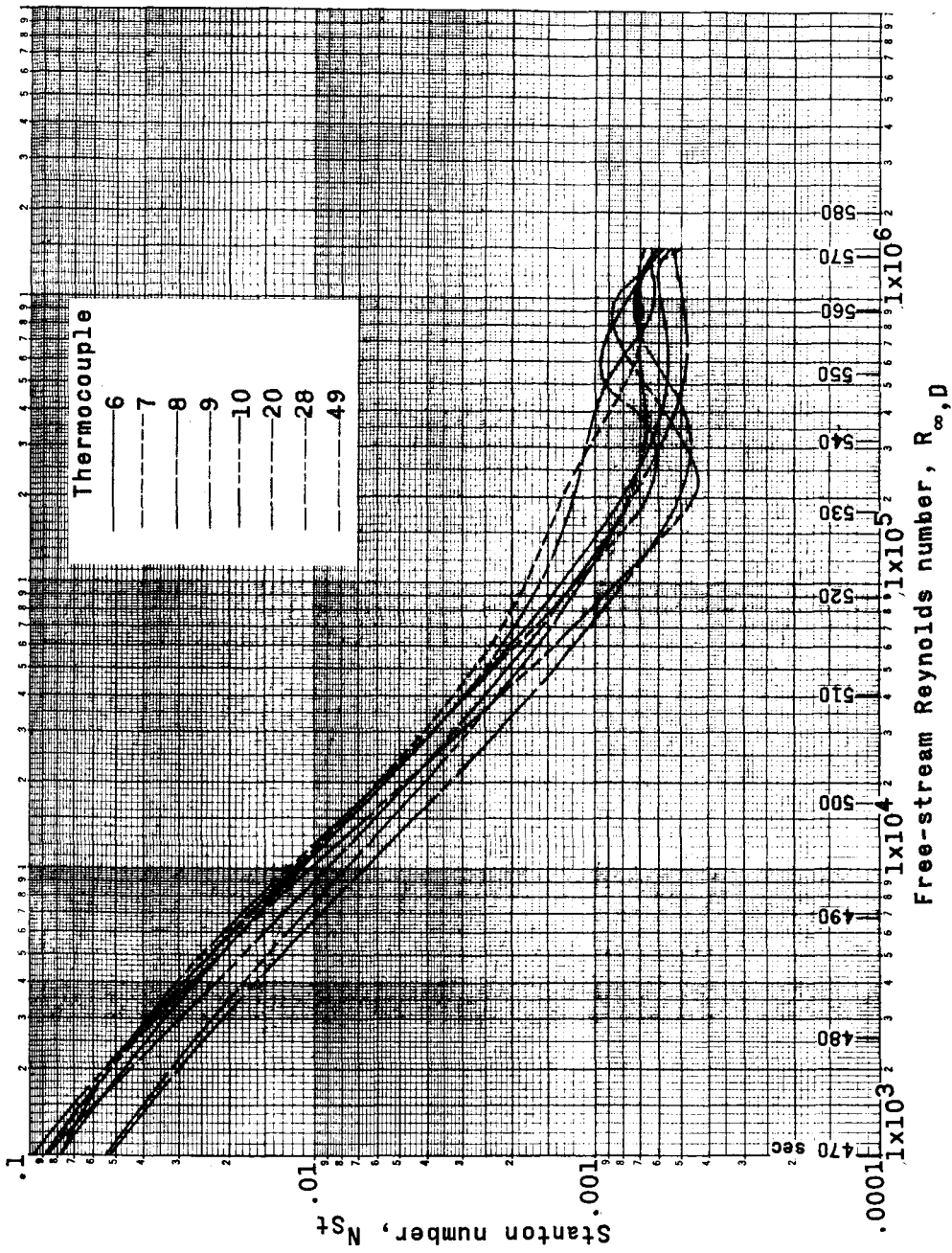


Figure 16. - Continued.



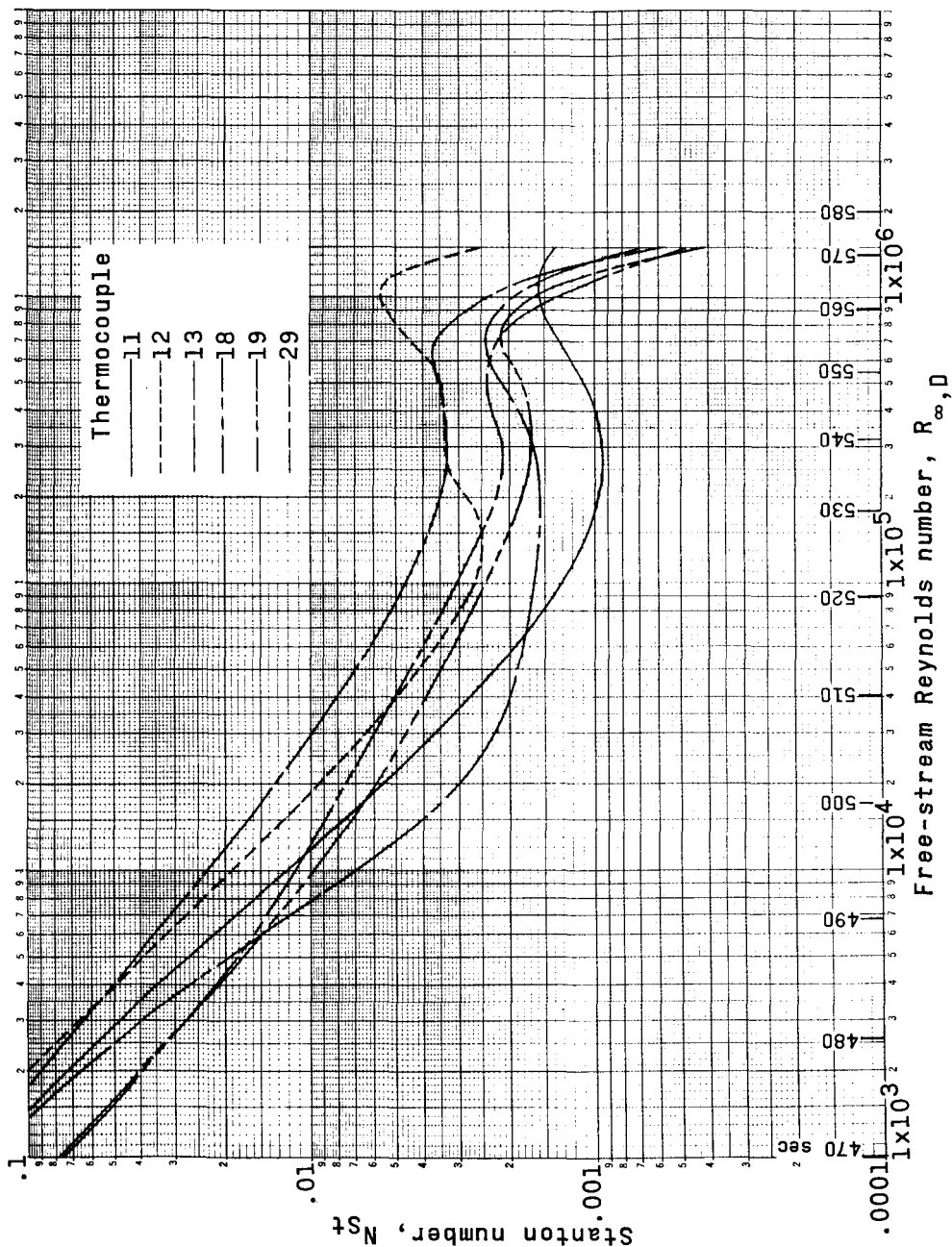
(a) Concluded.

Figure 16.- Continued.



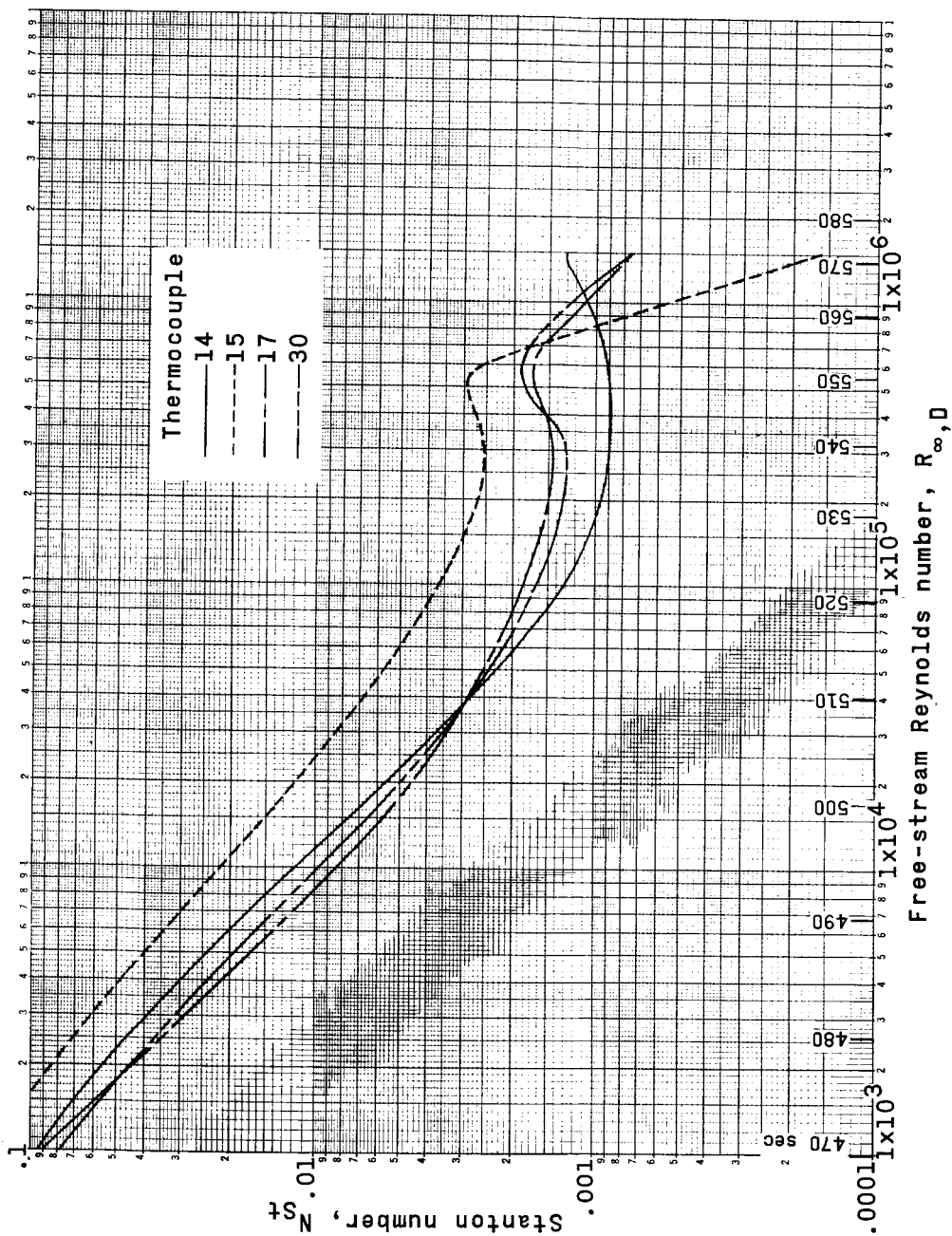
(b) Cone sidewall.

Figure 16.- Continued.



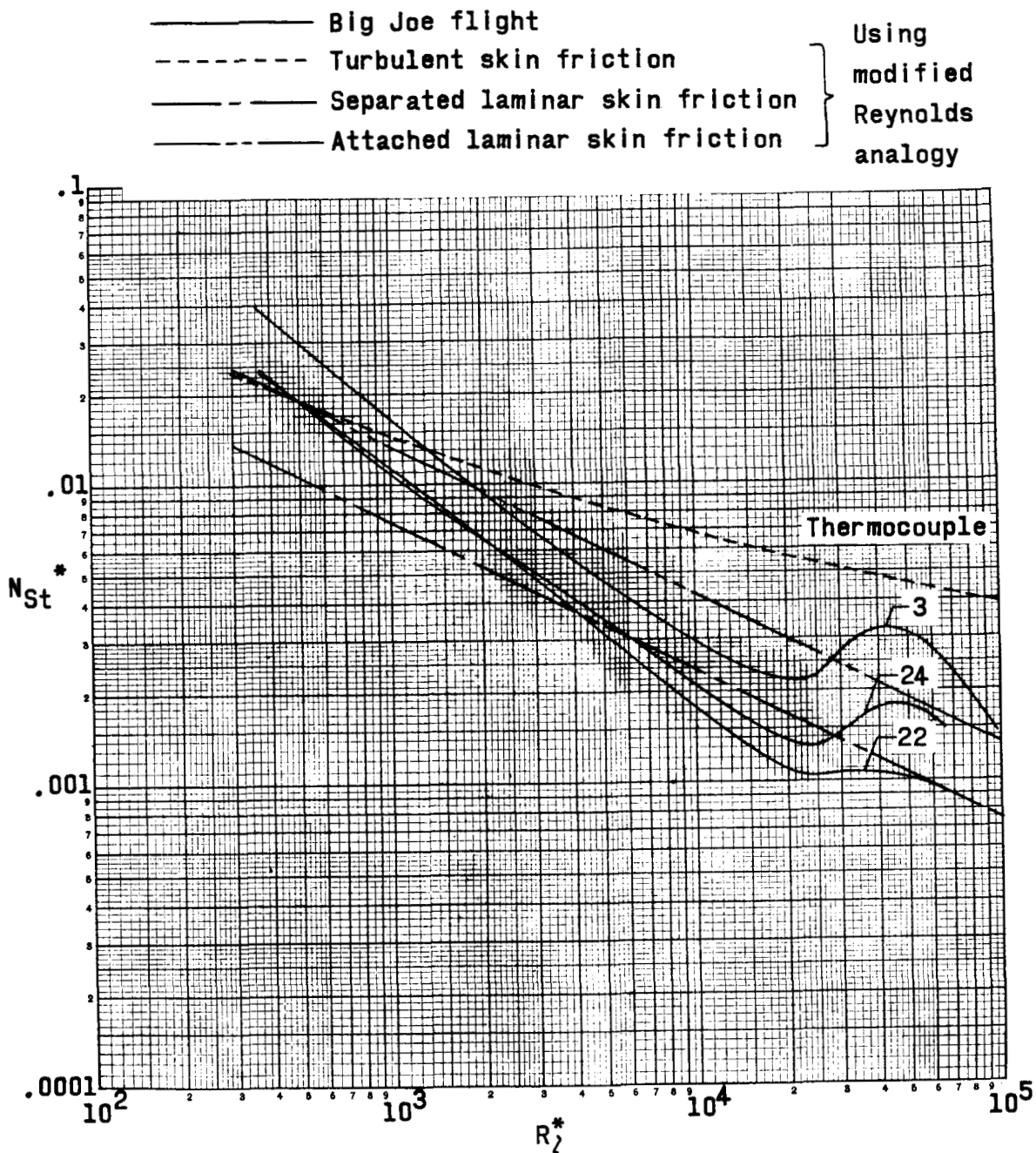
(c) Cylinder.

Figure 16.- Continued.



(d). Top canister.

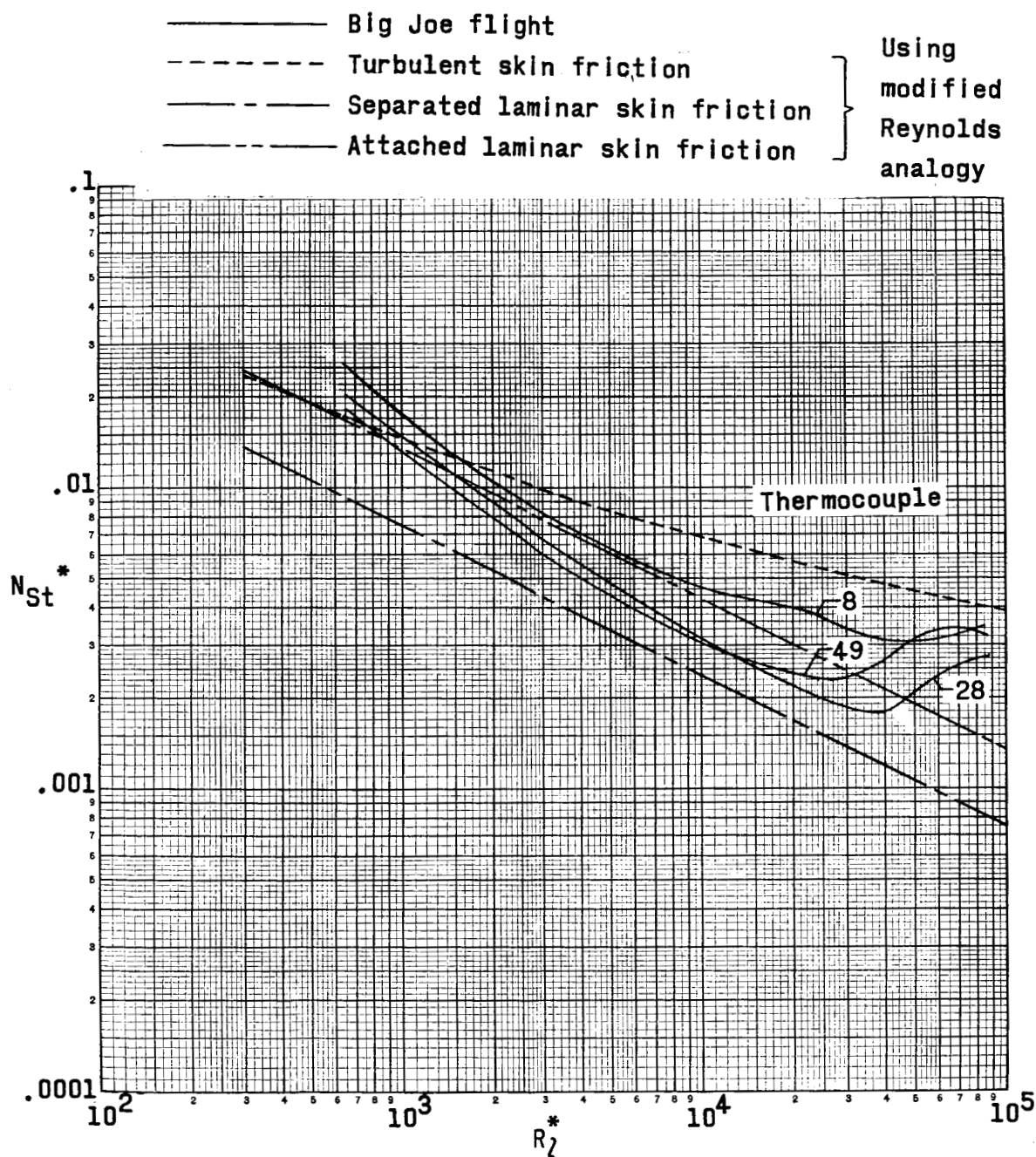
Figure 16.- Concluded.



(a) Middle station on pressure vessel sidewall.

Figure 17.- Comparisons of experimental and theoretical Stanton numbers.

DECLASSIFIED

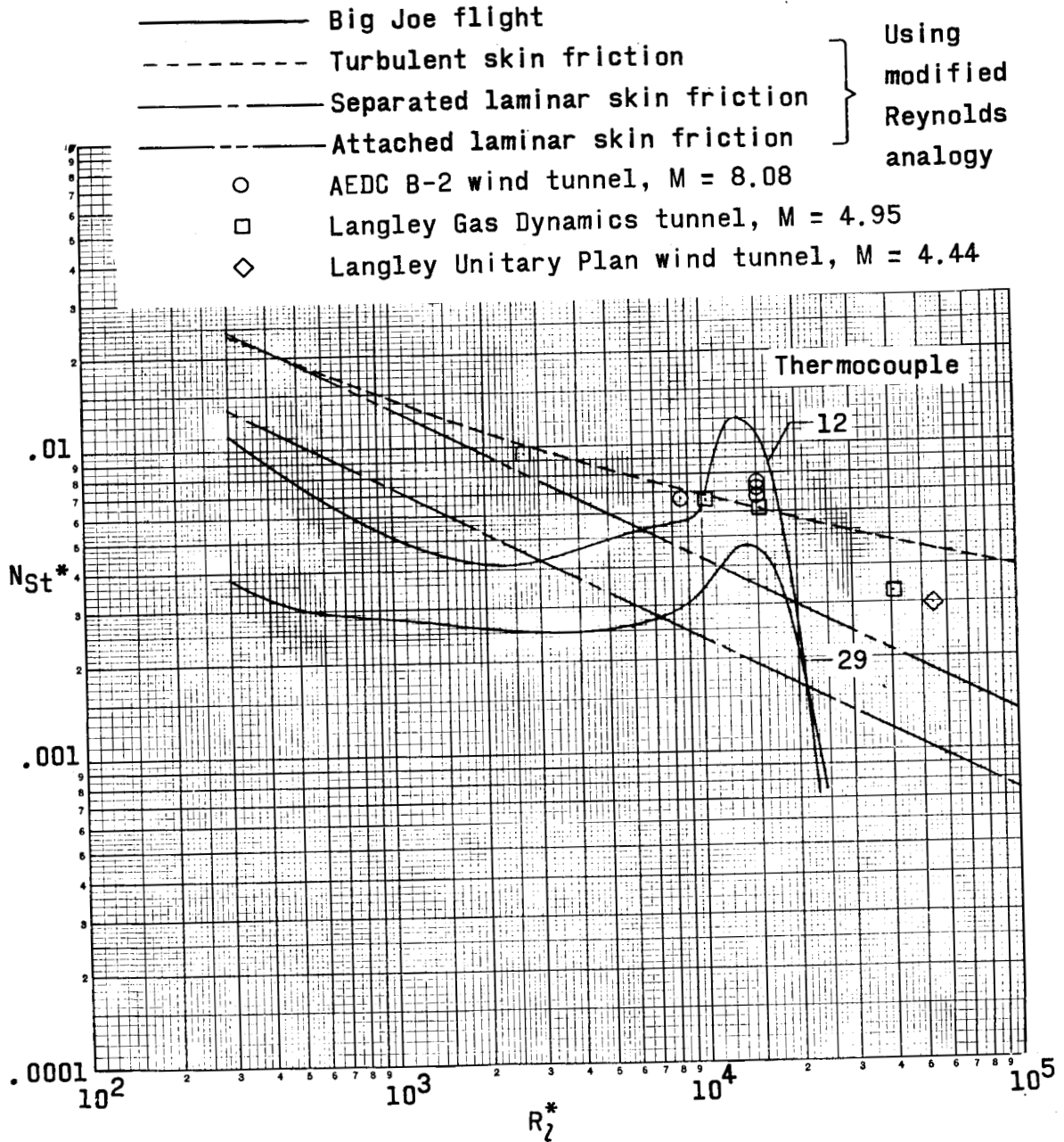


(b) Middle station on conical section.

Figure 17.- Continued.

03171220 1030

50



(c) Middle station on cylinder.

Figure 17.- Concluded.